

# Timanide (Ediacaran–Early Cambrian) Metamorphism at the Transition from Eclogite to Amphibolite Facies in the Beloretsk Complex, SW-Urals, Russia


Arne P. Willner<sup>1,2\*</sup>, Michael Gopon<sup>1</sup>, Johannes Glodny<sup>3</sup>, Victor N. Puchkov<sup>4</sup>, Hans-Peter Schertl<sup>1,2</sup>

1. Institute of Geology, Mineralogy and Geophysics, Ruhr-University Bochum, D-44780 Bochum, Germany

2. College of Earth Science and Engineering, Shandong University of Science and Technology, Qingdao 266590, China

3. Deutsches Geoforschungszentrum GFZ, Telegrafenberg, 14473 Potsdam, Germany

4. Institute of Geology and Geochemistry, Uralian Branch of Russian Academy of Science, 620016 Ekaterinburg, Russia

 Arne P. Willner: <https://orcid.org/0000-0002-8195-0635>

**ABSTRACT:** The Beloretsk Metamorphic Complex in the SW Urals formed at a convergent eastern margin of Baltica during the Neoproterozoic–Early Cambrian Timanide orogeny. It comprises three major units with lenses of facies-critical metabasites within metasedimentary rocks: A lowermost eclogite unit, an intermediate garnet amphibolite unit and an upper amphibolite-greenschist unit. Pressure (*P*)-temperature (*T*)-paths of four rocks from the two lowermost units were determined mainly by *PT* pseudosection techniques showing similar clockwise loops at different peak metamorphic, water-saturated conditions: A phengite-bearing eclogite shows peak *PT* conditions of 16.5–18.5 kbar/525–550 °C (stage I) followed by stage II at 11.5–13.0 kbar/585–615 °C. A garnet amphibolite from the intermediate unit yields lower peak conditions of 11.7–14.5 kbar/480–510 °C (stage I) followed by stage II at 9.5–11.0 kbar/535–560 °C. However, a granite gneiss in the eclogite unit shows similar maximum pressures as the eclogite, but higher temperatures at 15.6–16.2 kbar/660–675 °C, whereas a garnet micaschist contains comparable high pressure relicts, but underwent an advanced midcrustal reequilibration at 7.5–9.0 kbar/555–610 °C. We dated the eclogite by a 7-point Rb/Sr mineral isochron (phengite, omphacite, apatite) at 532.2±9.1 Ma interpreted as age of crystallisation of the eclogitic peak *PT* assemblage. This age is the youngest compared to the known Timanide metamorphic and magmatic ages.

**KEY WORDS:** Urals, eclogite, high pressure metamorphism, Timanide orogeny, Rb-Sr dating, *PT* pseudosections, *PT*-path.

## 0 INTRODUCTION

High pressure (HP) metamorphic rocks, particularly eclogite and related rocks, are important for understanding the tectonic evolution of collisional wedges along the suture zones of collisional orogens or subduction channel rocks along convergent margins. HP rocks in the Urals formed during three major orogenic episodes (Fig. 1; summary in Puchkov, 2013, 2010): (1) During Ediacaran–Early Cambrian times the Timanide orogeny resulted in a change from passive margin conditions during most of the Proterozoic to convergent margin conditions at the eastern side of the Baltica protocontinent. (2) During the Devonian the Uralide orogeny represented a continent-arc collision with an Early Paleozoic arc that had been separated from Baltica earlier. (3) The final accretion of the composite Kazakh-Kyrgyz Middle Paleozoic paleocontinent in the East Uralian zone occurred

during the Carboniferous. Whereas Devonian HP rocks are widespread along the Uralide suture zone (main Uralian fault; Fig. 1) and as yet intensively studied (summary in Brown et al., 2006), little is known about Carboniferous HP rocks in the East Uralian zone or on Ediacaran–Early Cambrian HP rocks in the west of the Ural-Tau fault, where effects of the Timanide orogeny can be studied (Fig. 1). In this work we focus on eclogite and related HP rocks within the so-called Beloretsk Metamorphic Complex (BMC; Figs. 1, 2; Alekseev et al., 2009, 2006; Glasmacher et al., 2001; Alekseev, 1984), where an eclogite occurrence is known near the town of Beloretsk within a metamorphic terrain mostly affected by the Timanide orogeny. The as yet unknown age of the eclogite could potentially be crucial for reconstructions for Late Neoproterozoic to Cambrian plate movements.

Here we attempt for the first time to quantitatively derive peak metamorphic conditions and partial *PT*-paths for four selected HP rocks of the BMC, an eclogite, a garnet amphibolite, a granite gneiss and a garnet micaschist as well as to obtain a first age of the peak metamorphic conditions of the eclogite. We follow two major questions: What is the nature of the transition from lower pressure garnet amphibolite to eclogite? Did the eclogite form “*in situ*” with respect to its neighbouring rocks?

\*Corresponding author: [arne.willner@rub.de](mailto:arne.willner@rub.de)

© China University of Geosciences (Wuhan) and Springer-Verlag GmbH Germany, Part of Springer Nature 2019

Manuscript received June 21, 2019.

Manuscript accepted September 15, 2019.

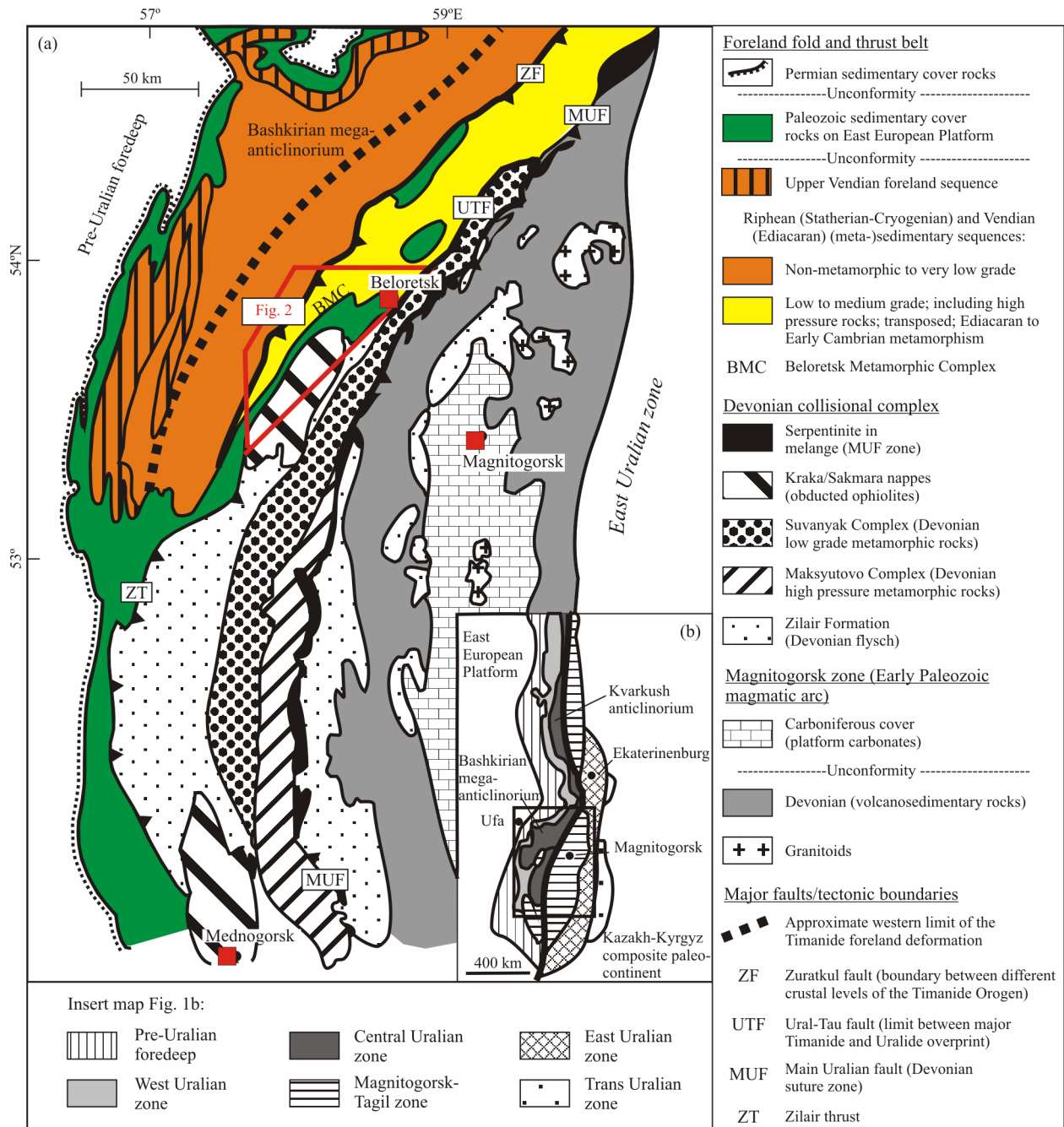


**Figure 1.** (a) Geological map of the southwestern Urals (modified after Brown et al., 2006, 1998; information from Puchkov, 2010 is included); (b) geological zones in the Urals.

**1 GEOLOGICAL SETTING AND PREVIOUS GEOCHRONOLOGY**

The Beloretsk Metamorphic Complex is situated at the southwestern end of a low to medium grade metamorphic basement between the Ural-Tau and Zuratkul faults east of the Uralide foreland fold-and-thrust belt, the so-called Bashkirian mega-anticlinorium (BMA; Fig. 1). In the BMA of the southwestern Urals a 1.8–2.3 Ga old Paleoproterozoic basement is overlain by a 12–15 km thick, mainly siliciclastic sequence of Riphean (1 760±10 to ~630 Ma, Puchkov, 2013; Statherian-Cryogenian, Cohen et al., 2013) and Vendian (~630–542 Ma, Puchkov, 2013; ~635–542 Ma, Semikhatov et al., 1991; Ediacaran, Cohen et al., 2013) sedimentary rocks deposited within

the extensive Bashkirian Basin (Puchkov, 2013, 1997). Sedimentation occurred at a stable continental margin of eastern Baltica until the end of the Early Vendian at ~610–620 Ma, when a change to active margin conditions was marked by a pronounced change of type and derivation of detritus in Upper Vendian sediments (Puchkov, 2013, 2010; Willner et al., 2002, 2001; Maslov et al., 1997). The onset of Upper Vendian clastic foreland sedimentation (Fig. 1) marks the beginning of the Timanide orogeny in the SW Urals (Puchkov, 2013). This foreland sedimentation during the ongoing Timanide orogenic event is corroborated by <sup>40</sup>Ar/<sup>39</sup>Ar ages of 590–630 Ma of detrital orthoclase in unmetamorphosed sandstone derived from an eastern (present day coordinates) source (Glasmacher et al.,

2001) as well as by finds of Ediacaran Metazoa (Kolesnikov et al., 2015) and a  $548 \pm 8$  Ma U-Pb age of zircon from a tuff layer of the uppermost Zigan Formation (Grazhdankin et al., 2011).  $^{40}\text{Ar}/^{39}\text{Ar}$  white mica spot ages of detrital phengite in Upper Vendian sedimentary rocks derived from the BMC yielded 571–609 Ma (Willner et al., 2004). The absolute age of deposition of the entire Upper Vendian foreland sequence (Basu, Kukkarauk and Zigan formations) is  $\sim 610$ –542 Ma (Puchkov et al., 2014; Puchkov, 2013).

Immediately west of the Zuratkul fault the supracrustal Riphean and Vendian sedimentary rocks were weakly deformed and overprinted at diagenetic to very low grade conditions (Matenaar et al., 1999; Fig. 1). However, east of the Zuratkul fault metamorphism in the BMC abruptly increases to mainly medium grade conditions overprinting rocks with a penetrative transposition foliation and accompanying three ductile deformation events with a predominant vergence towards the SSW (Glasmacher et al., 2001; Giese et al., 1999). By lithological comparison the rocks of the BMC were traditionally mapped as metamorphic equivalents of Riphean and Vendian sedimentary rocks including Mesoproterozoic bimodal mafic-felsic dykes, which also occur unmetamorphosed or with very low grade metamorphic overprint west of the Zuratkul fault (Puchkov, 2013; Alekseev et al., 2009, 2006; Sobolev et al., 1968).

Two important protolith ages are known so far in the BMC (Fig. 2a): U/Pb dating of zircon in the weakly gneissose Achmerovo granite by Krasnobaev et al. (2008) yielded an intrusion age of  $1\,381 \pm 23$  Ma (upper discordia intercept) with a weakly constrained later overprint at  $565 \pm 200$  Ma (lower discordia intercept). Earlier a Pb/Pb evaporation age of zircon in the Beloretzk eclogite of  $\sim 1\,350$  Ma was interpreted by Glasmacher et al. (2001) as the crystallisation age of an igneous protolith. Both protolith ages correspond to the 1 380–85 Ma Mashak event of bimodal mafic-felsic dyke intrusions that widely affected the entire Riphean Basin along the eastern margin of Baltica (Puchkov et al., 2013). The Mashak event marks the beginning of Middle Riphean (1 400–1 030 Ma) sedimentation and represents a major rift event possibly related to the break-up of the Columbia supercontinent (Puchkov et al., 2013). The occurrence of this bimodal magmatism as metamorphic equivalents in the BMC proves (1) that the crust of the BMC is definitely Baltican crust and not an “exotic” terrane and (2) that the eclogite formed *in situ* from basaltic dyke precursors within a thinned passive margin. Trace element geochemistry supports this rift setting: The Achmerovo granite and related granitoids plot into “within plate” fields in tectonic discrimination diagrams (Shardakova, 2016; Alekseev et al., 2009). The BMC eclogite and amphibolite show chondrite-normalized REE pattern similar to P-MORB with enriched LREE (Alekseev et al., 2009; Galieva, 2004).

Penetrative transposition foliation  $S_1$  parallel to the original layering gently dips to the NNE throughout the BMC (Glasmacher et al., 2001). This foliation is locally cut by mylonitic SW-NE trending, sinistral transtensive shear zones with top-down-to-NW kinematics. A third ductile deformation is characterised by NNE-SSW trending east-vergent folds (Glasmacher et al., 2001). Systematic occurrence of different metabasic rocks such as eclogite, garnet amphibolite and amphibolite/greenschist which are characteristic for pressure-sensitive metamorphic fa-

cies (eclogite, albite-epidote amphibolite and amphibolite/greenschist facies) allows to subdivide the BMC tentatively into three major units with increasing pressure from the NNE to the SSW (Figs. 2a, 2b). Likely this stack represents a tilted crustal section or, alternatively, a continental convergence-related stack of nappes. The structurally lowermost eclogite unit contains eclogite lenses showing variable retrograde amphibolitization intercalated within marble and some garnet micaschist and micaschist. Important minor rock types are the local occurrence of the Achmerovo granite gneiss and a rare finding of a talc-kyanite assemblage (Galieva, 2004). The intermediate garnet amphibolite unit comprises mainly garnet micaschist with intercalations of garnet amphibolite lenses. The uppermost amphibolite-greenschist unit is characterised by the widespread occurrence of micaschist, quartzite, graphitic schist, amphibole-bearing schist with amphibolite bodies of variable size and local greenschist occurrences.

First attempts to derive peak  $PT$  conditions for the Beloretzk eclogite were made by Alekseev (1984) and Alekseev et al. (2009) using conventional geothermobarometry. Results were  $520$ – $540$  °C/9–10 kbar and  $620$ – $650$  °C/9–13 kbar, respectively. However, derived pressures are only minimum conditions, as the albite-jadeite-quartz-barometry was applied.

First isotopic ages related to the metamorphic overprint in the BMC were K/Ar ages of white mica concentrates within the wide range of 510–635 Ma (Matte et al., 1993; Harris, 1977; Lennykh, 1968). More robust ages were provided by Glasmacher et al. (2001) who derived six  $^{40}\text{Ar}/^{39}\text{Ar}$  plateau ages of white mica concentrates ranging from  $541 \pm 3$  to  $597 \pm 4$  Ma in the structurally lower part of the BMC (Fig. 2a). However, at that time these ages were interpreted as cooling ages. A similar interpretation of a single  $^{40}\text{Ar}/^{39}\text{Ar}$  age of a metasomatic amphibole at  $718 \pm 5$  Ma led Glasmacher et al. (2001) to the contradictory suggestion that cooling under  $\sim 500$  °C would even have occurred prior to the Timanide event. This would demand an even older age of eclogite metamorphism and an exotic nature of the BMC, because there was ongoing sedimentation within the Riphean Basin at that time.

Exhumation, surface uplift and erosion of the BMC likely ended at  $\sim 490$  Ma, when uppermost Cambrian(?)–Tremadocian to Middle Ordovician clastic sediments with intercalated subalkaline lava flows and tuffs were deposited on the pronounced unconformity on the top of the BMC and the slightly deformed Riphean–Lower Vendian sedimentary rocks further west (Puchkov, 2013, 2010). This is followed by spreading of the pre-Uralian ocean during the Arenigian and thus the beginning of the Uralide orogenic cycle. It should be noted that the BMC as a crystalline block at the surface was only affected by some brittle deformation during the Uralide orogeny. This contrasts with the Riphean/Vendian sedimentary sequences in the BMA west of the Zuratkul fault, which got their most pronounced deformational imprint as a west-vergent fold-and-thrust-belt during the Uralide event. This is also the cause for the apparent change of vergence on both sides of the Zuratkul fault (Glasmacher et al., 2001; Giese et al., 1999).

## 2 ANALYTICAL METHODS

Mineral compositions were determined using a Cameca

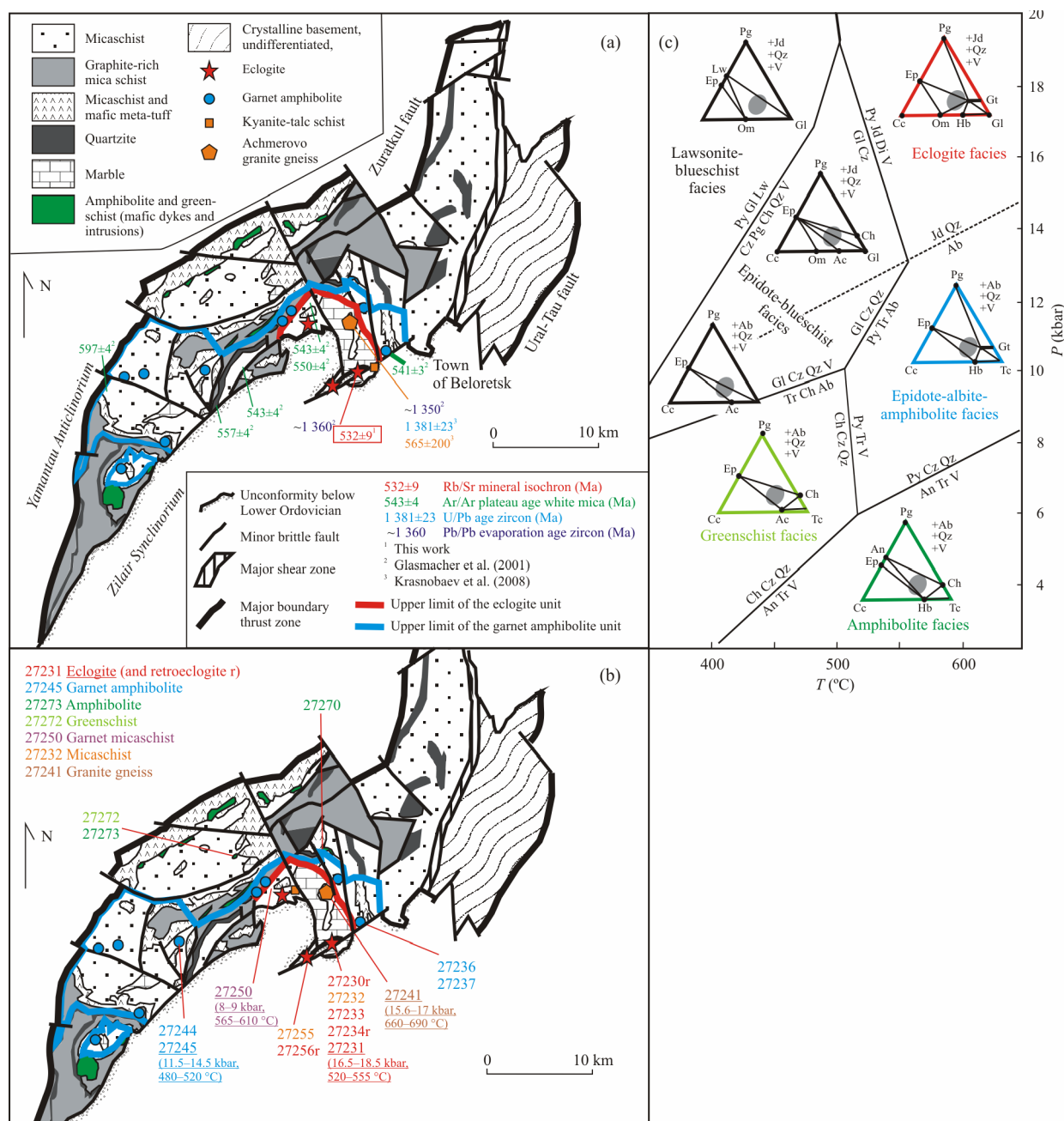


**Figure 2.** (a) Lithological map of the Beloretsk Metamorphic Complex (redrawn and modified by Glasmacher et al. (2001) after Shvetsov (1980)). The metamorphic information is from Alekseev personal communication (1999) and Alekseev et al. (2009, 2006); geochronological information is included; (b) sample localities and peak metamorphic conditions of four studied samples; (c) general petrogenetic grid with selected limiting multivariant reactions defining boundaries of low- and medium-grade facies. As shown they were calculated with common intermediate activities of solid solution end-members in the system CNMASH by Evans (1990).

SX 50 electron microprobe at Ruhr-Universität Bochum, Germany. Operating conditions were an acceleration voltage of 15 kV, a beam current of 15 nA, 20 s counting time per element on peak and background and a defocused beam of 5 μm diameter. Standards used were synthetic pyrope (Si, Al, Mg), rutile (Ti), glass of andradite composition (Ca, Fe), jadeite (Na), spessartine (Mn), K-bearing glass (K), Ba-silicate glass (Ba, La). The PAP procedure was used for matrix correction. Element distribution images of garnet were acquired with a beam current of 40 nA and an acceleration voltage of 15 kV. Images were obtained in stage scan mode at a step width of 2 μm per pixel and a measurement

time of 140 ms per pixel. Analyses and structural formulae of minerals were calculated using the software MINCALC-V5 (Bernhardt, 2010) and are presented together with the calculation procedure of the structural formulae in ESM1.

Whole rock major element compositions were acquired by X-ray fluorescence (XRF) on a Philips PW2404 at Ruhr-Universität Bochum. Required glass disks were prepared by fusing the ground sample powder mixed with Spectromelt® in a ratio of 10 : 1. FeO contents were determined by titration, CO<sub>2</sub> by IR-spectroscopy and H<sub>2</sub>O by loss on ignition.

Rb/Sr isotopic data were generated at GeoForschungs Zen-



trum Potsdam/Germany using a Thermo Scientific TRITON thermal ionization mass spectrometer. Sr was measured in dynamic multicollection mode and Rb isotope dilution analysis was done in static multicollection mode. The  $^{87}\text{Sr}/^{86}\text{Sr}$  obtained for NIST SRM 987 reference material during the period of analytical work was  $0.710\,255 \pm 0.000\,005$  ( $2\sigma_m$ ;  $n=23$ ). For age calculation, standard uncertainties of  $\pm 0.005\%$  for  $^{87}\text{Sr}/^{86}\text{Sr}$  and of  $\pm 1.5\%$  for  $^{87}\text{Rb}/^{86}\text{Sr}$  ratios were assigned to the results. All individual analytical uncertainties were smaller than these values. Handling of mineral separates and analytical procedures are described in more detail in Glodny et al. (2008). Uncertainties of isotope and age data are quoted at  $2\sigma$ . The program ISOPLOT (Ludwig, 2009) was used to calculate regression lines. The  $^{87}\text{Rb}$  decay constant is the one recommended by Villa et al. (2015).

### 3 RESULTS

#### 3.1 Petrographical Characteristics and Mineral Compositions

Our description of petrographical characteristics and mineral compositions concentrates on the four facies-critical metabasitic rocks (eclogite, garnet amphibolite, amphibolite and greenschist) as well as on some selected rocks from the eclogite unit such as garnet micaschist, micaschist and granite gneiss. The list of the assemblages in the rock samples is given in Table 1.

##### 3.1.1 Eclogite and retro-eclogite

Macroscopically, the eclogite (samples 27231, 27233) is

medium to fine-grained. Grain sizes of amphibole and mica are generally a little larger than those of garnet and omphacite. Major mineral constituents and respective modal amounts are garnet (30%–40%), omphacite (5%–25%), phengite (from accessory amounts up to 15%), quartz (<5%) and amphibole (<5%). In retrogressively altered samples (retro-eclogite samples 27230, 27234, 27256), the amount of amphibole can reach 50% and epidote as well as carbonate are becoming major constituents. Rutile (<3%), biotite, chlorite, titanite and magnetite are accessories. Eclogite samples are generally undeformed, but in retro-eclogite samples occasionally small volume portions are characterized by a weak foliation.

Common inclusions in garnet (grain size 0.5–0.8 mm) are epidote, rutile, amphibole, quartz and clinopyroxene; often large phengite grains form inclusions in the core of garnet that is radially fractured (Figs. 3a, 3b). Garnet may exhibit reaction rims of amphibole ( $\pm$ epidote and biotite). Garnet shows similar compositional variations in eclogite and retro-eclogite (Fig. 4a). For sample 27231 an element distribution map of garnet is provided in Fig. 4d and its full compositional range is as follows:  $\text{And}_{0.013-0.017}\text{Grs}_{0.34-0.35}\text{Alm}_{0.53-0.55}\text{Sps}_{0.017-0.022}\text{Prp}_{0.08-0.10}$  in the core to  $\text{And}_{0.007-0.014}\text{Grs}_{0.19-0.29}\text{Alm}_{0.50-0.54}\text{Sps}_{0.009-0.011}\text{Prp}_{0.18-0.25}$  at the rim. Mg-content strongly increases from the core towards the rim, whereas Ca- and Mn-contents decrease notably and Fe-contents decrease rather weakly.

Omphacite occurs in grain sizes of 0.05–0.3 mm. It is often elongated and weakly aligned and occasionally exhibits

**Table 1** Assemblages and characteristics of samples in the BMC

	Garnet	Amphibole	Epidote	Chlorite	White mica	Biotite	Clinopyroxene	K-feldspar	Albite	Plagioclase	Quartz	Rutile	Titanite	Ilmenite	Magnetite	Calcite	Deformation
Eclogite and retroeclogite																	
27231	x	x	x	x	x		x	x	x	x	x	x	x		x		nd
27233	x	x	x		x		x				x	x	x		x	x	nd
27234	?	x		x	x	x	?				x	x	x		x	x	vwf
27230	x	x	x		x	x	?				x	x	x		x	x	vwf
27256	?	x					?				x	x	x		x	x	vwf
Garnet amphibolite																	
27236	x	x	x	x					x		x			x		x	sf
27237	x	x	x	x		x			x		x			x		x	nd
27244	x	x				x			x		x			x			nd
27245	x	x	x	x		x			x		x	x	x	x		x	nd
Amphibolite																	
27273		x	x	x		x					x		x		x		nd
Greenschist																	
27272		x	x	x					x		x		x				sf
Garnet micaschist																	
27250	x			x	x	x				x	x	x					s
Micaschist																	
27255				x	x	x					x	x	x		x	x	s
27232		x		x	x	x				x	x		x		x		s
Granite gneiss																	
27241	x		x		x	x		x	x		x		x				wgn

nd. not deformed; s. schistose; wgn. weakly gneissose; vwf. very weakly foliated; sf. strongly foliated.

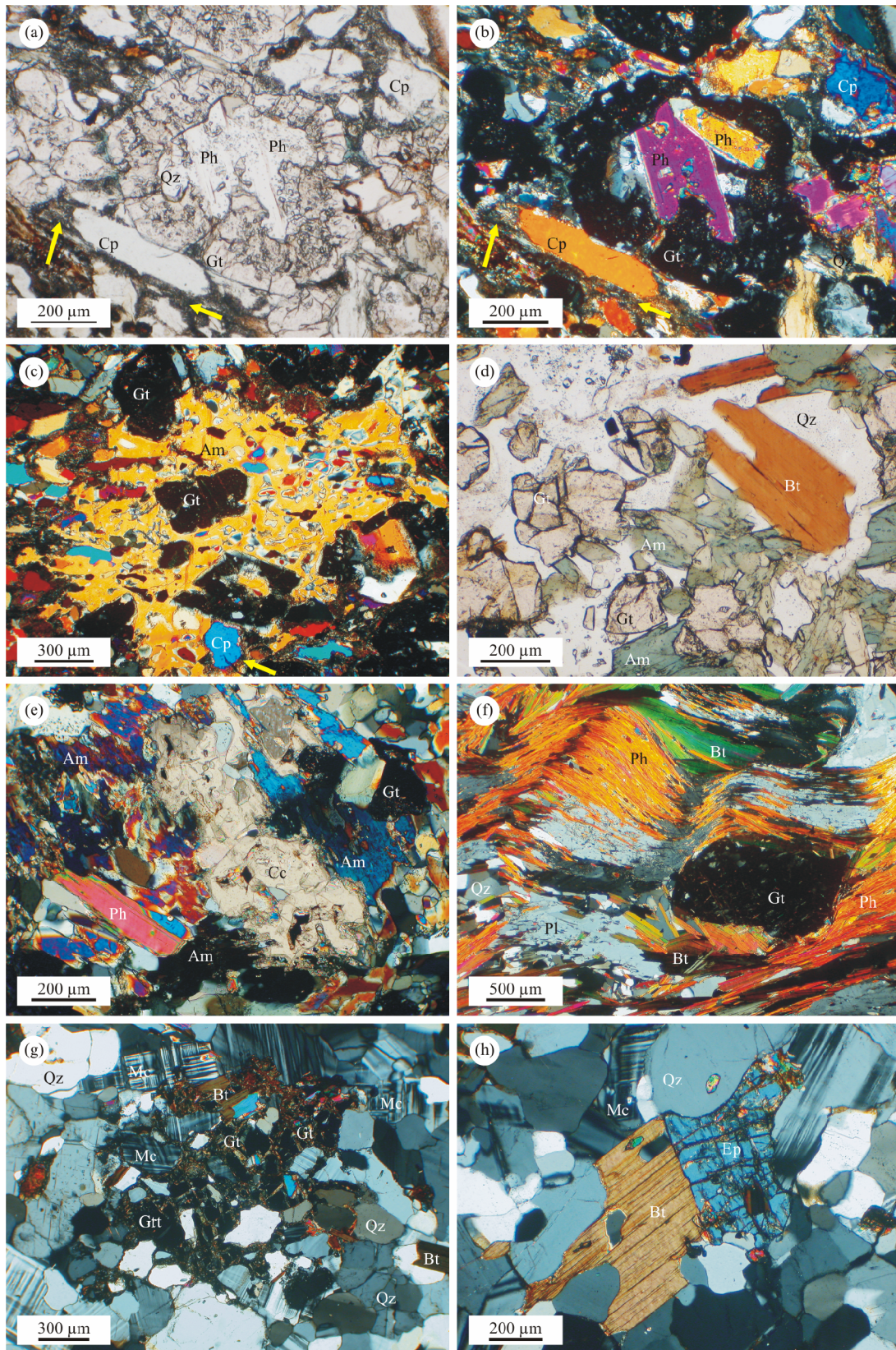


**Figure 3.** Microphotographs of rock samples studied. (a) Garnet (Gt) with phengite (Ph) inclusions in omphacite (Cp)-rich matrix of eclogite sample 27231; arrows indicate amphibole-rich symplectites (plane polarized light PPL); (b) same as (a) under crossed polars (XPL); (c) coarse-grained amphibole 3 (Am) with inclusions of Gt and Cp (eclogite sample 27231; XPL); (d) Gt-Am-quartz (Qz)-biotite (Bt) matrix (garnet-amphibolite sample 27245; PPL); (e) calcite (Cc)-bearing portion of the matrix (garnet-amphibolite sample 27245; XPL); (f) Gt porphyroblast in a matrix rich in Bt, Ph, Qz, Pl (plagioclase porphyroblast; garnet micaschist sample 27250; XPL); (g) sieve structure of Gt in a matrix rich in Qz, Mc (microcline), Bt (granite gneiss sample 27241; XPL); (h) Bt-epidote intergrowth texture in matrix rich in Qz and Mc (granite gneiss sample 27241; XPL).



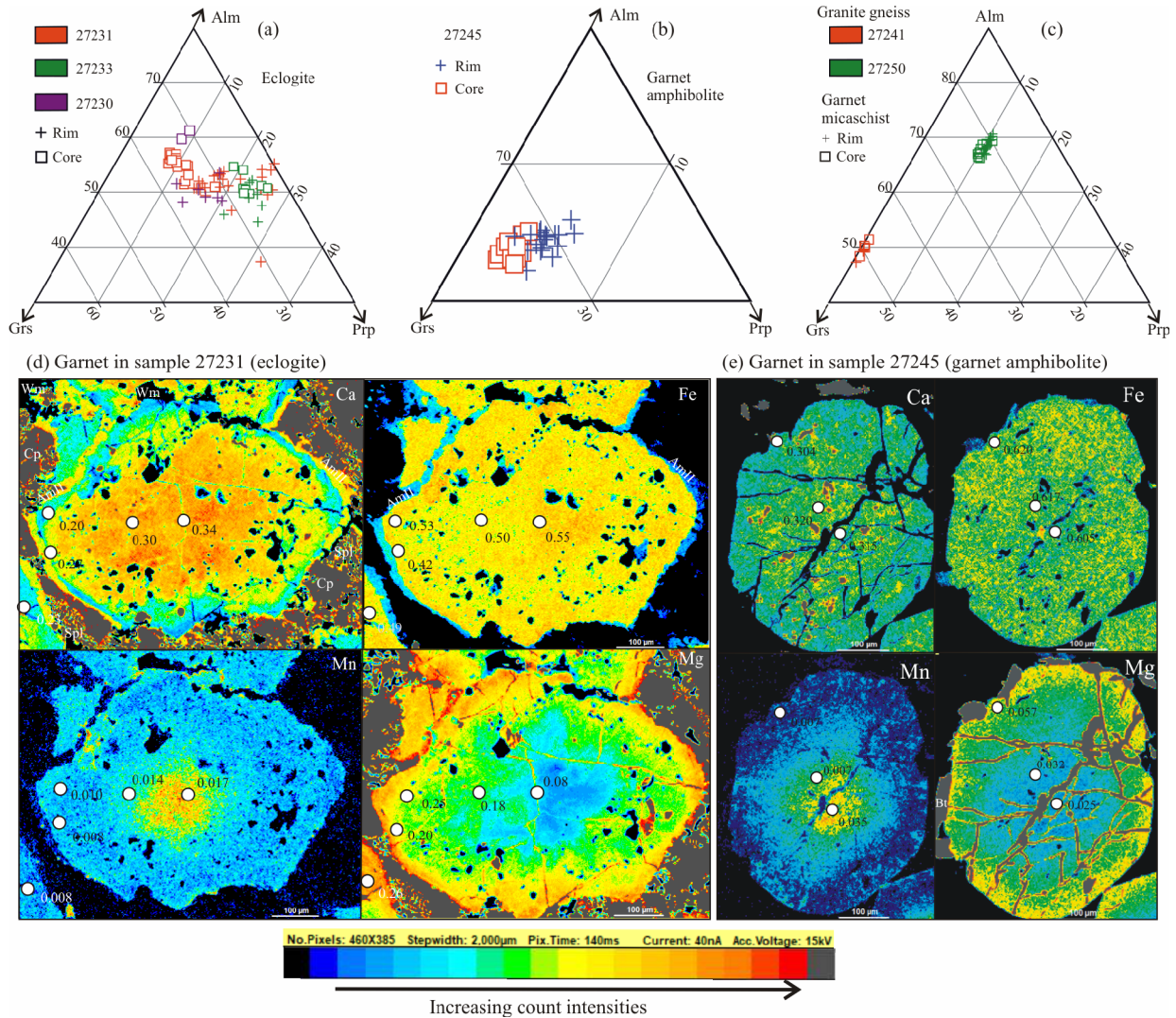


**Figure 4.** (a)–(c) Compositional variations of garnet cores and rims in almandine-pyrope-grossular triangular plots; (d) element distribution maps of garnet in eclogite sample 27231; (e) element distribution maps of garnet in garnet amphibolite sample 27245.

amphibole-rich symplectitic rims. Omphacite occurs as matrix crystals, inclusions in garnet and in symplectite, all of which are different in composition (Fig. 5). The matrix omphacite has an average composition of 60.7 mol% diopside, 38.5 mol% jadeite and 0.8 mol% acmite components. Two out of 16 analyses lack a detectable acmite component. A chemical zoning pattern was not observed. Omphacite in symplectites has an average composition of 78.6 mol% diopside, 20.3 mol% jadeite and 3.2 mol% acmite component similar to those of inclusions in garnet and coexists with plagioclase with variable compositions (74.9 mol%–93.1 mol% albite, 6.5 mol%–24.8 mol% anorthite and 2 mol%–4 mol% orthoclase components).

In general, three types of amphibole occur: Am I is fine-grained and forms inclusions in garnet, Am II is either part of the symplectitic rims around garnet or present in the matrix. Am III is coarse-grained (1–1.5 mm) and overgrew garnet, quartz, phengite and omphacite during a later stage (Fig. 3c). While in the rock matrix garnet and omphacite often exhibit reaction rims due to later retrogression, inclusions of garnet and clinopyroxene in Am II are lacking these rims, indicating a formation of Am II prior to the retrogression of garnet and om-

phacite. Only if eclogite shows an intense retrogression and thus is characterized by high amounts of Am III, a fourth amphibole generation (Am IV) is observed which forms either gridded intergrowth textures with uneven extinctions, or idioblastic crystals <100 µm.

The four generations of amphibole also differ by compositions as can be shown in classification diagrams according to Hawthorne et al. (2012; Figs. 6a, 6b). Amphibole can be assigned either to the calcium or sodium-calcium subgroup, but most of Am I and II are also characterized by high occupation of the A-position (>0.50 apfu). Whereas all amphibole generations show similar ranges of minor elements and oxidation stages (Ti 0.00–0.07 apfu, exceptionally 0.36 apfu, Mn 0.00–0.04 apfu,  $X_{\text{Fe}^{3+}} = \text{Fe}^{3+}/(\text{Fe}^{3+} + \text{Fe}^{2+})$  0.01–0.68, exceptionally 0.85), strong differences are between Am I and II versus Am III and IV with respect to contents of Si,  $^{\text{B}}\text{Na}$ ,  $^{\text{A}}\text{Na}$  and  $X_{\text{Mg}} = \text{Mg}/(\text{Mg} + \text{Fe}^{2+})$  as shown in the following.

Am I inclusions yield compositions corresponding to pargasite, sadanagaite, tschermakite or to winchite with Si 5.79–6.64,  $^{\text{B}}\text{Na}$  0.27–0.57,  $^{\text{A}}\text{Na}$  0.16–0.74 apfu and  $X_{\text{Mg}}$  0.36–0.39.

Am II shows a similar composition, but a more limited

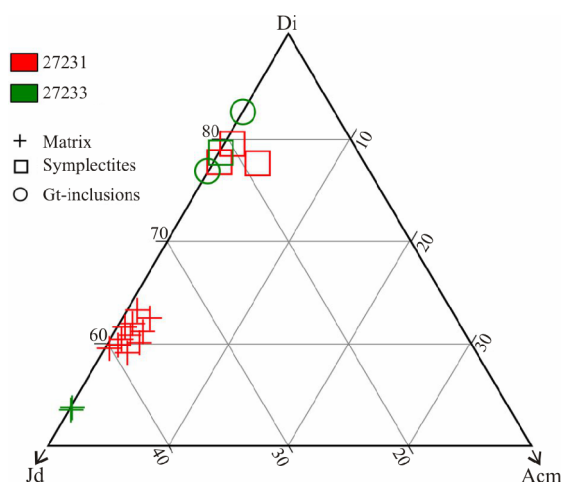


**Figure 5.** Compositional variations of omphacite generations in eclogite samples within a jadeite-diopside-acmite triangular plot.

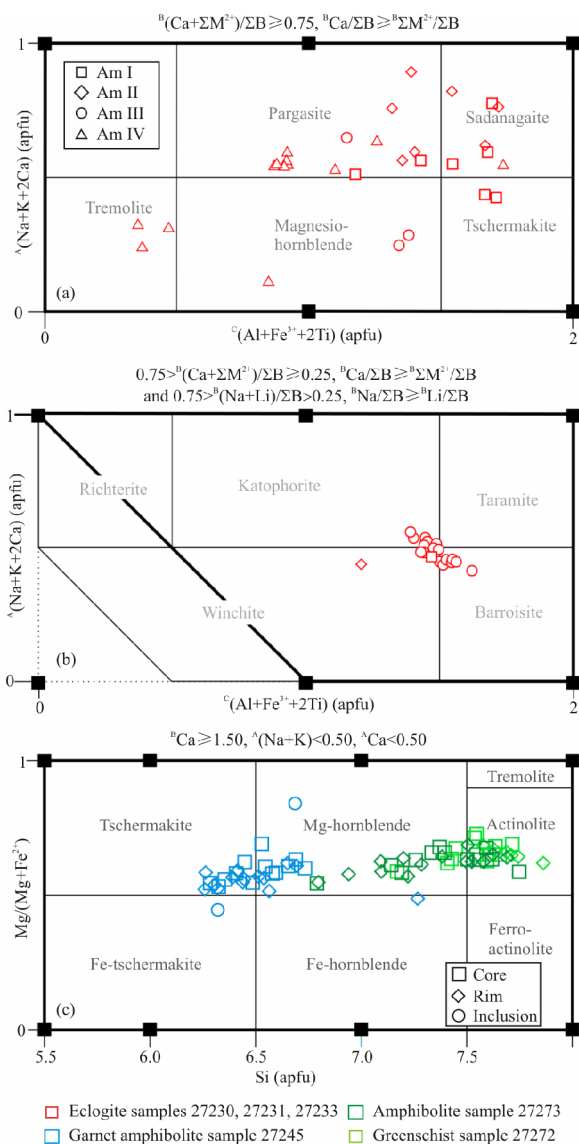


**Figure 6.** (a) Compositional variations of amphibole generations in eclogite samples on the basis of the nomenclature of Hawthorne et al. (2012); (b) compositional variations of amphibole in garnet amphibolite, amphibolite and greenschist samples following the nomenclature by Leake et al. (1997).

range that comprises pargasite and sadanagaite with Si 5.64–6.53, <sup>B</sup>Na 0.13–0.43, <sup>A</sup>Na 0.00–0.66 apfu and *X*<sub>Mg</sub> 0.46–0.61.

Larger amphibole (Am III) is classified as magnesian-hornblende, winchite, barroisite or katophorite with Si 6.59–6.88, <sup>B</sup>Na 0.38–0.68, <sup>A</sup>Na 0.10–0.50 apfu and *X*<sub>Mg</sub> 0.72–0.89.

Am IV has the widest compositional range. Most of the analyses are classified as tremolite and pargasite, but some grains as magnesian-hornblende, sadanagaite or tschermakite. This amphibole generation comprises the following compositional ranges: Si 6.12–7.84, <sup>B</sup>Na 0.00–0.44, <sup>A</sup>Na 0.00–0.43 apfu and *X*<sub>Mg</sub> 0.64–0.73. A significant chemical zoning could not be observed in neither generation.

White mica (grain size <0.6 mm) occurs in the matrix and often shows small cryptocrystalline reaction rims. It forms inclusions in garnet (see above) and Am III. Fine-grained white mica forms intergrowth textures with Am IV. White mica composition is phengite (i.e., ≥3.2 Si apfu; Rieder et al., 1998; Fig. 7a) showing similar variations of Si-contents (3.25–3.40 Si apfu) between samples and little deviation from the ideal Tschermak substitution 2Al=Si+(Mg+Fe<sup>2+</sup>) due to Fe<sup>3+</sup>-substitution in some grains (calculated Fe<sup>3+</sup> 0.00–0.25 apfu) and minor di/trioctahedral substitution. *X*<sub>Mg</sub> (=Mg/(Mg+Fe<sup>2+</sup>)) varies from 0.56 to 0.81. Na-contents (0.06–0.20 apfu) may rise up to 0.62 in retro-eclogite samples. Contents of Ba (≤0.026 apfu), Ti (0.002–0.091 apfu) are minor.

Rutile up to 100 μm forms inclusions in garnet and clusters in the matrix. Occasionally it is enveloped by rims of titanite. Epidote, titanite and carbonates are accessories, their modal proportion, however, increases in retrogressively altered eclogite.

### 3.1.2 Garnet amphibolite

Garnet amphibolite is the typical metabasite of the unit that structurally overlies the eclogite unit (Fig. 2) and it can

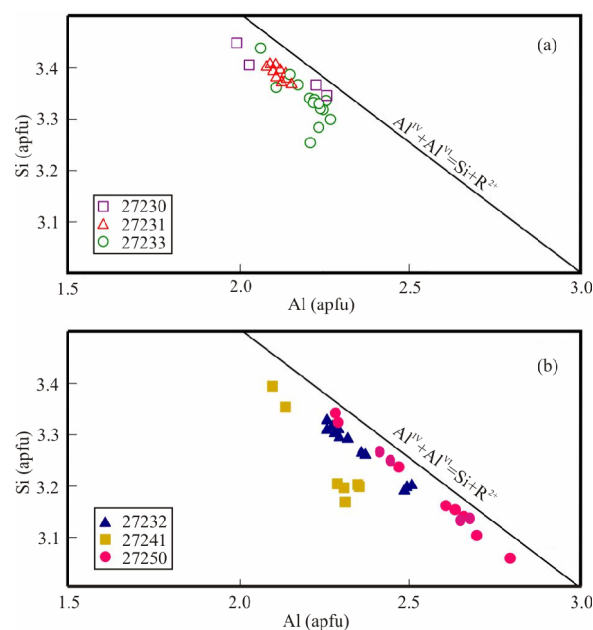


**Figure 7.** Variations of Si apfu with Al apfu in potassic white mica. The line of the ideal Tschermak's substitution is indicated. (a) Eclogite samples 27230, 27231, 27233; (b) micaschist sample 27232, granite gneiss sample 27241, garnet micaschist sample 27250.



easily be distinguished from retro-eclogite by different mineral assemblages and compositions. Except for sample 27236, samples 27237, 27244 and 27245 are undeformed, fine-grained and dark greenish grey in color. Garnet, albite and biotite porphyroblasts are a few mm in size and thus can be macroscopically identified. Except for granoblastic textures in undeformed portions, rare banded intercalations of oriented greenish and whitish-grey layers (sample 27236) can be observed.

The following assemblage is documented: amphibole (45%), garnet (5%–20%), quartz (5%–30%), albite (~20%; in undeformed variety only), biotite (<5%; in undeformed variety only), epidote (5%–20%), ilmenite (up to 10%); accessories are chlorite, apatite, titanite and calcite. This characteristic assemblage points to conditions of the epidote-albite-amphibolite facies (Fig. 2c).

In undeformed portions of the rock, garnet is generally fine-grained, isometrical and roundish and 0.2–0.5 mm in size. Within the layered intercalations (sample 27236), the grain size of garnet is 1.5–4 mm. Whereas in the greenish, amphibole-dominant layers garnet forms isometrical shapes, the quartz- and chlorite-dominant layers exhibit sieve-like structures of garnet. Many garnet grains show parallel sets of fractures documenting brittle deformation. Inclusions of epidote, amphibole, titanite, ilmenite and rare rutile are observed in garnet. A typical photomicrograph showing intergrowth textures of amphibole, garnet, and biotite in a quartz-rich matrix is presented in Fig. 3d. Typical compositional variations of garnet in garnet amphibolite sample 27245 are  $\text{And}_{0.012-0.034}\text{Grs}_{0.313-0.357}\text{Alm}_{0.582-0.622}\text{Sps}_{0.009-0.060}\text{Prp}_{0.022-0.041}$  in the core to  $\text{And}_{0.008-0.014}\text{Grs}_{0.281-0.307}\text{Alm}_{0.620-0.633}\text{Sps}_{0.005-0.014}\text{Prp}_{0.041-0.62}$  at the rim (see also Figs. 4b, 4e). From core to rim, Mg strongly and Fe weakly increase, whereas contents of Ca and Mn notably decrease. Mn shows a typical bell-shaped growth zonation.

Amphibole is idioblastic in shape, inclusion-free, intensively pleochroitic (with a typical hornblende colour absorption bluish-green to light green to light yellow) and occasionally zoned. Its grain size is about 50–100  $\mu\text{m}$  partly forming clusters of 1.2–2.5 mm size. In banded portions, the amount of amphibole varies widely. Whereas in the greenish layers (which are dominated by amphibole) the proportion reaches up to 70%, in whitish-grey layers (rich in chlorite and quartz) it is up to 30%. In the banded rocks (sample 27236) amphibole forms a lineation. Amphibole is invariably classified as magnesio-hornblende and tschermakite as shown in Fig. 6c. A chemical zoning could not be determined, although a core of lighter coloured pleochroism is observable in several grains.

The average grain size of quartz is 20  $\mu\text{m}$ . In granoblastic portions the amount of quartz reaches 5%, in layered portions 30%. In the layered portions a weak undulatory extinction is observed. Almost pure albite mostly forms xenoblastic, isometrical porphyroblasts 0.3–1.5 mm in size. These late porphyroblasts are rich in inclusions and envelope all earlier formed phases. Biotite occurs in undeformed portions of garnet amphibolite and forms flakes of 0.3–1 mm in size; occasionally it is partly replaced by chlorite. Biotite has an intermediate composition between phlogopite and annite ( $X_{\text{Mg}}$  0.49–0.55) with minor Ti 0.09–0.011, Mn <0.017, Ba 0.006–0.01 and Na 0.03–0.04 apfu.

In undeformed rocks, ilmenite which is typically associated with titanite, shows sieve-like structures. In the banded rock portions which are lacking titanite, ilmenite forms tabular

morphologies. Grain size is 0.4–0.6 mm. Epidote (<0.5 mm) may occur as a major constituent (<20%) or as an accessory phase in undeformed garnet amphibolite; in the banded sample portions modal abundances are about 5%. Rare calcite in the amphibole-rich matrix is shown in Fig. 3e.

### 3.1.3 Amphibolite and greenschist

Two types of metabasite could be identified in the upper unit of the BMC, both characterized by the absence of garnet.

An undeformed coarse grained amphibolite (sample 27273) shows macroscopically visible amphibole grains up to 0.5 mm and amygdules (0.2–1 mm in size) in hand specimen. Main mineral constituents are amphibole (~50%) and epidote (45%), whereas biotite and retrograde chlorite are minor constituents and titanite, quartz and calcite are present as accessories.

Amphibole is strongly pleochroitic (bluish-green to green to light yellow). Its composition varies from magnesiohornblende to tschermakite (Fig. 6c) with following compositional variations: Si 6.78–7.74 apfu,  $X_{\text{Mg}}$  0.55–0.69,  $^{\text{A}}\text{Na}$ <0.30,  $^{\text{B}}\text{Na}$ <0.41, Ti<0.16, Mn 0.02–0.07 apfu. No compositional zonation was detected.

Epidote occurs as single grains, as local metasomatic monomineralic clusters and as fillings of amygdules. It is weakly pleochroitic (pale yellow-colourless) and its average grain size is about 0.5 mm.  $\text{Fe}^{3+}$  content is 0.48–0.52 apfu and slightly decreases from core to rim. Biotite occurs occasionally as flakes of 0.3–0.5 mm in size with a slightly Fe-rich composition ( $X_{\text{Mg}}$  0.44–0.47). Like amphibole, biotite is often replaced by chlorite. The amphibolite sample lacks plagioclase, but its tschermakitic amphibole allows an assignment to the classical amphibolite facies.

By contrast, the strongly foliated metabasite (27272) of the upper BMC unit has a typical greenschist facies assemblage with chlorite, amphibole and epidote each in a modal abundance of ca. 20%. Abundant quartz and albite occur as further major constituents of around 10% each. Slightly greenish and oriented chlorite with anomalous interference colours ( $X_{\text{Mg}}$  0.49; Si 5.32–5.46 apfu) forms platy grains of a length of around 0.05–0.1 mm and defines a pronounced foliation as oriented amphibole. Weakly coloured amphibole grains are generally larger than chlorite grains with an average grain size of 0.5 mm. Individual crystals can reach sizes of up to 1 mm. Its composition varies from actinolite to magnesio-hornblende (Fig. 6c; Si 7.176–7.852 apfu,  $X_{\text{Mg}}$  0.58–0.72;  $^{\text{A}}\text{Na}$  <0.15,  $^{\text{B}}\text{Na}$  0.10–0.25, Ti 0.002–0.018, Mn 0.034–0.053 apfu). Epidote grains ( $\text{Fe}^{3+}$  0.45–0.52 apfu) have a relatively uniform size (around 0.1 mm) and mostly hypidiomorphic or nodular habits. Quartz and albite grains in polygonal aggregates and nodular aggregates of titanite have sizes of 0.1–0.5 mm and modal abundances of ~10% each. Apatite, zircon and opaque minerals occur as accessory phases.

### 3.1.4 Granite gneiss

The Achmerovo granite gneiss (sample 27241) from the eclogite unit basically consists of quartz, K-feldspar, biotite and plagioclase likely belonging to its magmatic precursor assemblage. In addition, white mica, garnet and epidote occur which are constituents formed during the metamorphic overprint. Weakly oriented micas define a faint foliation which is best

observed macroscopically. In detail, the list of modal amounts is as follows: quartz (30%), K-feldspar (30%), plagioclase (15%), biotite (15%); the metamorphic minerals white mica, garnet and epidote sum up to about 10%. Accessories are titanite, zircon and opaques.

Quartz yields a bimodal distribution with coarse grains (~500  $\mu\text{m}$ ) with intense undulatory extinction, and smaller grains (~100  $\mu\text{m}$ ) which are weakly undulatory. K-feldspar (average grain size of 400  $\mu\text{m}$ ) shows a cross-hatched twinning which is characteristic of microcline. The average grain size of plagioclase is around 500  $\mu\text{m}$ . Plagioclase is pure albite (<1 mol% anorthite component) showing that magmatic plagioclase was completely overprinted during metamorphism.

Biotite grains show a light olive-green to dark brown pleochroism and reach sizes of 2 mm. Biotite has an Fe-rich composition ( $X_{\text{Mg}}$  0.147–0.156), but enhanced Ti-contents (0.10–0.13 apfu).

Flakes of white mica reach 400  $\mu\text{m}$  in size. White mica is phengite with Si-contents ranging between 3.20 and 3.39 apfu (Fig. 7b). However, one grain was found to display an exceptionally high Si-content of 3.62 apfu. Further compositional ranges are as follows: calculated  $\text{Fe}^{3+}$ -contents 0.00–0.23 apfu,  $\text{Fe}^{2+}$  0.24–0.39 apfu, Mg 0.05–0.16 apfu,  $X_{\text{Mg}}$  (=Mg/(Mg+ $\text{Fe}^{2+}$ )) 0.15–0.33, Ti 0.00–0.02 apfu, Ba 0.00–0.03 apfu, Na 0.02–0.03 apfu.

Garnet up to 2 mm in size forms sieve structures and preferentially grew along grain boundaries of quartz and feldspar (Fig. 3g). Garnet zonation is little pronounced showing a range of end member compositions of  $\text{And}_{0.028-0.042}\text{GrS}_{0.400-0.412}\text{Alm}_{0.426-0.455}\text{SpS}_{0.099-0.118}\text{Prp}_{0.003-0.004}$  in the core and  $\text{And}_{0.024-0.034}\text{GrS}_{0.402-0.428}\text{Alm}_{0.422-0.445}\text{SpS}_{0.100-0.117}\text{Prp}_{0.004-0.005}$  at the rim. Only pyrope and grossular contents slightly increase from core to rim.

Epidote occasionally contains cores of allanite, typically occurs in assemblage with biotite and yields grain sizes of 50 to 400  $\mu\text{m}$ . Figure 3f shows intergrowth with biotite. Epidote has  $\text{Fe}^{3+}$ -contents of 0.70–0.74 apfu.

### 3.1.5 Garnet micaschist and micaschist

Macroscopically, garnet micaschist (sample 27250) within the eclogite unit is characterized by garnet porphyroblasts within a groundmass of pronouncedly oriented white mica. Major constituents are white mica (30%–40%), quartz (20%–30%), plagioclase (15%–25%), biotite (~15%), garnet (~10%) and chlorite (~5%); tourmaline and apatite are accessories.

Oriented flakes of white mica are 0.4–0.6 mm long and define the predominant cleavage. Smaller undeformed recrystallized grains occur at microfold hinges of a crenulation cleavage. White mica shows a remarkably wide range of compositions (Fig. 7b) from muscovite to phengite (Si 3.05–3.33 apfu) with  $X_{\text{Mg}}$  0.56–0.75, Ti 0.014–0.025 apfu and Na 0.085–0.184 apfu.

Biotite flakes (0.1–0.5 mm) are either mimetically aligned parallel to the direction of the major deformation characterized by white mica or are oriented randomly. Biotite has an intermediate composition between annite and phlogopite ( $X_{\text{Mg}}$  0.57–0.58) with Ti 0.06–0.08 apfu and Na 0.03–0.04 apfu.

Chlorite is light green in color; grain size and textural behaviour resemble biotite. Areas of large quartz grains (0.2–0.5

mm) exhibit an undulatory extinction and curved grain boundaries, whereas areas of fine grained quartz (average grain size of ~100  $\mu\text{m}$ ) exhibit straight grain boundaries and represent recrystallization structures.

Porphyroblastic plagioclase displays grains mimetically oriented parallel to the major deformation that is dominated by oriented mica and chlorite (Fig. 3f). It shows patchy extinction patterns and contains trails of biotite, chlorite, white mica, apatite, tourmaline and fluid inclusions. Albite twins are observed only rarely, saussuritisation is common. Plagioclase has 18 mol%–24 mol% anorthite component.

Garnet is 1.3–2 mm in size, typically yields poikilitic sieve structures and is surrounded by flakes of oriented biotite, white mica and chlorite (Fig. 3f). Inclusions are dominantly quartz and, to a lesser extent, also plagioclase and white mica. Occasionally inclusion trails define an earlier foliation. As particular inclusions in garnet chloritoid with an  $X_{\text{Mg}}$  of 0.25 was observed. Replacement textures of chlorite (in parts also of biotite) after garnet are common. Elemental zoning in garnet is less distinct than in the eclogite or the garnet amphibolite. Its end member compositions vary from  $\text{And}_{0.010-0.020}\text{GrS}_{0.200-0.232}\text{Alm}_{0.646-0.653}\text{SpS}_{0.020-0.045}\text{Prp}_{0.097-0.119}$  in the core to  $\text{And}_{0.010-0.020}\text{GrS}_{0.173-0.190}\text{Alm}_{0.681-0.73}\text{SpS}_{0.011-0.020}\text{Prp}_{0.109-0.113}$  at the rim showing faint increase of Mg and Fe and decrease of Mn and Ca from core to rim. Highest spessartine contents of 0.05 apfu can be observed in the outermost rim of garnet.

Garnet-free micaschist (sample 27232) from the eclogite unit shows similar characteristics as the garnet-micaschist. The amount of white mica, however, is higher and its grain size generally is smaller and uniformly around 100  $\mu\text{m}$ . Likewise grain size of quartz is smaller (50–100  $\mu\text{m}$ ). White mica is phengite (Si 3.20–3.33 apfu; Fig. 7b) with Ti 0.02–0.04 apfu, Na 0.03–0.04 apfu and  $X_{\text{Mg}}$  0.74–0.79. Biotite is similarly Mg-rich ( $X_{\text{Mg}}$  0.70–0.71) with Ti 0.06–0.07 apfu and Na 0.01–0.02 apfu. Plagioclase has 27 mol%–32 mol% anorthite component.

## 3.2 Geothermobarometry

For reconstruction of the *P-T* history we focussed on four critical rock samples: eclogite sample 27231, garnet amphibolite sample 27245, garnet micaschist sample 27250 and granite gneiss sample 27241. The latter two occur within the eclogite unit in close vicinity of eclogite occurrences. Mineral abbreviations used are as follows: Ab, albite; Am, amphibole; Ar, aragonite; Bt, biotite; Cc, calcite; Cd, chloritoid; Ch, chlorite; Cp, clinopyroxene; Do, dolomite; Ep, epidote; Gt, garnet; Im, ilmenite; Kf, potassic feldspar; Ky, kyanite; Lw, lawsonite; Mt, magnetite; Om, omphacite; Pa, paragonite; Ph, phengite; Pl, plagioclase; Qz, quartz; Rb, riebeckite; Ru, rutile; Sl, sillimanite; St, staurolite; Tt, titanite; V, H<sub>2</sub>O as hydrous fluid; Wm, potassic white-mica.

### 3.2.1 The applied methods

First four *PT* pseudosections and isopleths of mineral composition for the selected rock samples in the *PT*-range of 5–20 kbar, 400–700 °C were calculated using the PERPLE\_X software package (Connolly, 2005, 1990; latest version downloaded from www.perplex.ethz.ch). The thermodynamic data set of Holland and Powell (1998, updated 2002) for minerals and aqueous fluid was used. Calculations were performed using the following

solid-solution models: for white-mica, epidote, amphibole, garnet, plagioclase, omphacite, chloritoid, staurolite, carbonate, chlorite and biotite by Holland and Powell (2003, 1996) and Powell and Holland (1999). Only for eclogite the amphibole model by Diener et al. (2007) was applied. These models were selected from the distributed version of the PERPLE\_X solid-solution model file. Albite, K-feldspar, quartz, titanite, H<sub>2</sub>O and paragonite were considered as pure phases. The fluid equation of state used is a compensated Redlich-Kwong (CORK) by Holland and Powell (1998). For the calculation of the pseudosections the major element compositions analysed by XRF were simplified to a 11-component system (SiO<sub>2</sub>-TiO<sub>2</sub>-Al<sub>2</sub>O<sub>3</sub>-FeO-MgO-MnO-CaO-Na<sub>2</sub>O-K<sub>2</sub>O-H<sub>2</sub>O-O<sub>2</sub> and additional CO<sub>2</sub> for calcite-bearing sample 27245) and normalized to 100% (Table 2). Water contents were augmented to excess water conditions that are considered to have prevailed during peak *PT*-conditions. The amount of O<sub>2</sub> used was the one extracted from the original analyses. The amount of CaO was corrected for the amount of CaO present in apatite.

This forward modeling method has the advantage that (1) phase relationships can be predicted over a wide *PT*-field, (2) peak *PT* conditions can be directly extracted by comparison with the observed mineral assemblage in the studied rock, (3) parts of *PT*-paths can be derived by compositional isopleth intersections e.g., for garnet core and rims or with compositional isopleths of other minerals within the *PT* field of the observed assemblage, and (4) evidence for the form of the retrograde *PT* path can be extracted. The disadvantage of the method is that retrograde phases do not grow from the effective whole rock composition and hence tend not to be correctly represented in the *PT* pseudosection. For garnet rim compositions of the eclogite sample 27231 convergence of isopleths were rather wide. Hence we calculated equilibria by intersection of multivariant equilibria using the software winTWQ (Berman, 1991) based on the database of Berman (1988) in the system NCKFMASH. We used the databases DEC06.SLN and DEC06.DAT and calculated activities for the end members anorthite, almandine, pyrope, grossular,

tremolite and clinozoisite for garnet rims in contact with amphibole, plagioclase and epidote. Albite, quartz and water were treated as pure phases. The list of the calculated equilibria and the graphical representation is given in ESM2.

### 3.2.2 Results from thermodynamic calculations

#### 3.2.2.1 Eclogite (sample 27231)

The *PT* pseudosection calculated for eclogite sample 27231 (Figs. 8a–8c) shows a relatively wide *PT* field for the observed peak metamorphic assemblage garnet-omphacite-chlorite-white mica-epidote-quartz-rutile within the *PT* range of 11–18 kbar, 490–560 °C (Fig. 8a). This field is close to the limits of the *PT* fields of lawsonite (towards higher pressure), epidote (towards higher temperature), rutile (towards lower temperature; Fig. 8c), and amphibole (towards lower pressure). The latter confirms the observed retrograde nature of amphibole in this eclogite. However, albite, plagioclase and biotite would occur at much lower pressures than the peak *PT* metamorphic conditions derived. Intersection of isopleths of four garnet end members (Fig. 8b) for the range of garnet core compositions show optimal intersection within the higher *PT* part of the observed assemblage just below the isopleth of the maximum Si content (3.40 apfu) in phengite. This overlap and additionally the isopleths of the range of Na-contents (0.34–0.37 apfu) in the omphacite narrow the *PT* conditions during growth of the garnet core to 16.5–18.5 kbar/520–555 °C, which represents the peak pressure conditions (stage I).

According to the inclusions in garnet (quartz, mainly tschermakitic to pargasitic amphibole, low-Na clinopyroxene, epidote, phengite, rutile) with compositions similar to those of the later symplectite stage garnet overgrew an assemblage that had formed at elevated temperature and lower pressure. However, it is unlikely that the inclusion assemblage represents a prograde assemblage, because garnet cores nucleated at peak pressures and garnet cores are relatively free of inclusions. The isopleths for the garnet rim compositions do not yield reasonable intersections.

**Table 2** (a) Whole rock analyses and (b) simplified compositions for the calculation of *PT* pseudosections

(a)	27231	27245	27241	27250	(b)	27231	27245	27241	27250
SiO <sub>2</sub>	47.5	44.6	69.5	59.2	SiO <sub>2</sub>	46.5	44.1	69.6	59.4
TiO <sub>2</sub>	1.37	2.71	0.39	0.72	TiO <sub>2</sub>	1.34	2.68	0.39	0.72
Al <sub>2</sub> O <sub>3</sub>	13.8	13.5	11.9	18.6	Al <sub>2</sub> O <sub>3</sub>	13.5	13.4	11.9	18.7
Fe <sub>2</sub> O <sub>3</sub>	1.42	2.40	1.16	1.26	FeO	11.7	16.1	2.82	5.06
FeO	10.7	14.1	1.77	3.91	MnO	0.20	0.28	0.06	0.05
MnO	0.20	0.28	0.06	0.05	MgO	6.68	5.33	0.27	3.15
MgO	6.81	5.38	0.27	3.14	CaO	10.7	8.29	0.74	1.11
CaO	11.1	8.81	0.81	1.24	Na <sub>2</sub> O	2.13	1.93	3.04	2.05
Na <sub>2</sub> O	2.17	1.95	3.04	2.04	K <sub>2</sub> O	0.54	0.37	5.14	3.81
K <sub>2</sub> O	0.55	0.37	5.13	3.80	CO <sub>2</sub>		0.81		
P <sub>2</sub> O <sub>5</sub>	0.12	0.32	0.05	0.10	H <sub>2</sub> O	6.50	6.50	5.89	5.88
CO <sub>2</sub>		0.82			O <sub>2</sub>	0.15	0.20	0.11	0.12
LOI		0.97	0.62	2.75	Sum	100.0	100.0	100.0	100.0
Sum	95.6	96.2	94.7	96.9					

LOI. Loss of ignition.

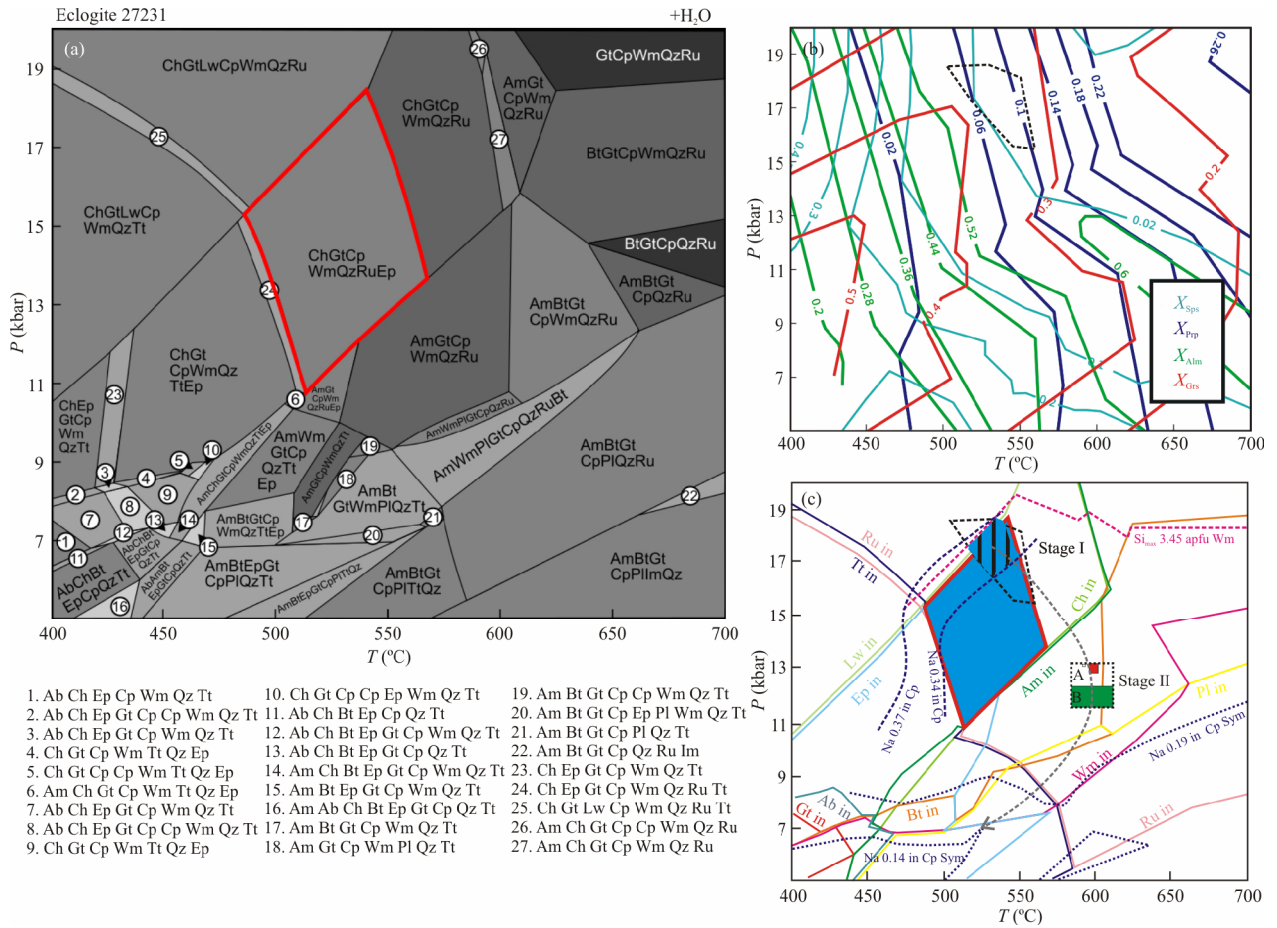


**Figure 8.** (a) *PT* pseudosection of the Beloretzk eclogite sample 27231 in the system  $\text{SiO}_2\text{-TiO}_2\text{-Al}_2\text{O}_3\text{-FeO-MgO-MnO-CaO-Na}_2\text{O-K}_2\text{O-H}_2\text{O-O}_2$ . Shading of *PT* fields from white towards dark grey represents increasing variance from bivariant, trivariant, quadrivariant, quintvariant to six-variant assemblages. The field of the observed peak metamorphic assemblage is marked in red. (b) Isopleths of garnet end member fractions. The stippled field marks the optimal convergence for the garnet core compositions. (c) *PT* fields of single mineral phases. *PT*-path defined by stage I (vertically ruled field) with the overlap of garnet core compositions, the compositional range of omphacite and the field of the observed assemblage, stage II by garnet rim compositions calculated (A) by conventional phengite-garnet-clinopyroxene geobarometry and (B) by multivariant reaction including symplectite compositions and by fields and finally by fields of retrograde assemblages.

They merely point to higher temperature during growth of the garnet rim. Instead we calculated a *PT* point at approximately 13 kbar, 600 °C (Fig. 8c, point A) by conventional geothermobarometry (clinopyroxene-garnet thermometer of Krogh Ravn (2000); garnet-clinopyroxene-phengite barometry of Waters and Martin (1993)) using adjacent rim compositions of garnet and phengite. Multivariant reactions were calculated using the winTWQ software for adjacent amphibole and garnet rim compositions and symplectitic clinopyroxene and plagioclase. Nineteen reactions of three independent equilibria intersect at 600±15 °C and 12±0.5 kbar (point B in Fig. 8c; see ESM2). Both points are close within the general error range of ~±1 kbar, ~±25 °C at 1σ level assumed for any geothermobarometry method (Spear, 1993). Hence the range of 11.5–13.0 kbar, 585–615 °C for stage II at peak temperature conditions gives an approximate range for the end of garnet growth and beginning of symplectite formation, when the *PT* path had reached the *PT*-field of amphibole. However, isopleths of Na-contents of symplectitic clinopyroxene (0.14–0.19) do not intersect this *PT*-range, but plot at lower pressure. This is likely due to the fact that the whole rock composition is not the effective one anymore for retrograde

reactions. Nevertheless these isopleths can further limit the geometry of the retrograde *PT*-path. This late partial *PT* path is characterized by slight decompression and cooling into the *PT*-fields, where plagioclase, biotite and titanite are present. They occur as minor late phases and titanite frequently forms tiny rims around rutile (Fig. 8c).

### 3.2.2.2 Garnet amphibolite (sample 27245)

The best approach for the field of the observed assemblage in the *PT* pseudosection calculated for garnet amphibolite sample 27245 (Fig. 9a) is the field of the calculated assemblage garnet-amphibole-(riebeckite)-biotite-chlorite-epidote-carbonate-titanite in the *PT*-range of 11.5–14.5 kbar, 480–520 °C. Here albite does not appear, confirming the observed retrograde nature of albite as late porphyroblasts. In the *PT* pseudosection albite appears only below 9 kbar and 500 °C. The calculated “riebeckite” is an artefact that appears in some calculated assemblages at temperatures below 500 °C due to bad adaptation of  $\text{Fe}^{3+}$  in the chosen solution model. Nevertheless the field of the observed assemblage is well restricted as it is close to the upper temperature and lower pressure limit of the *PT* field of omphacite, the lower temperature



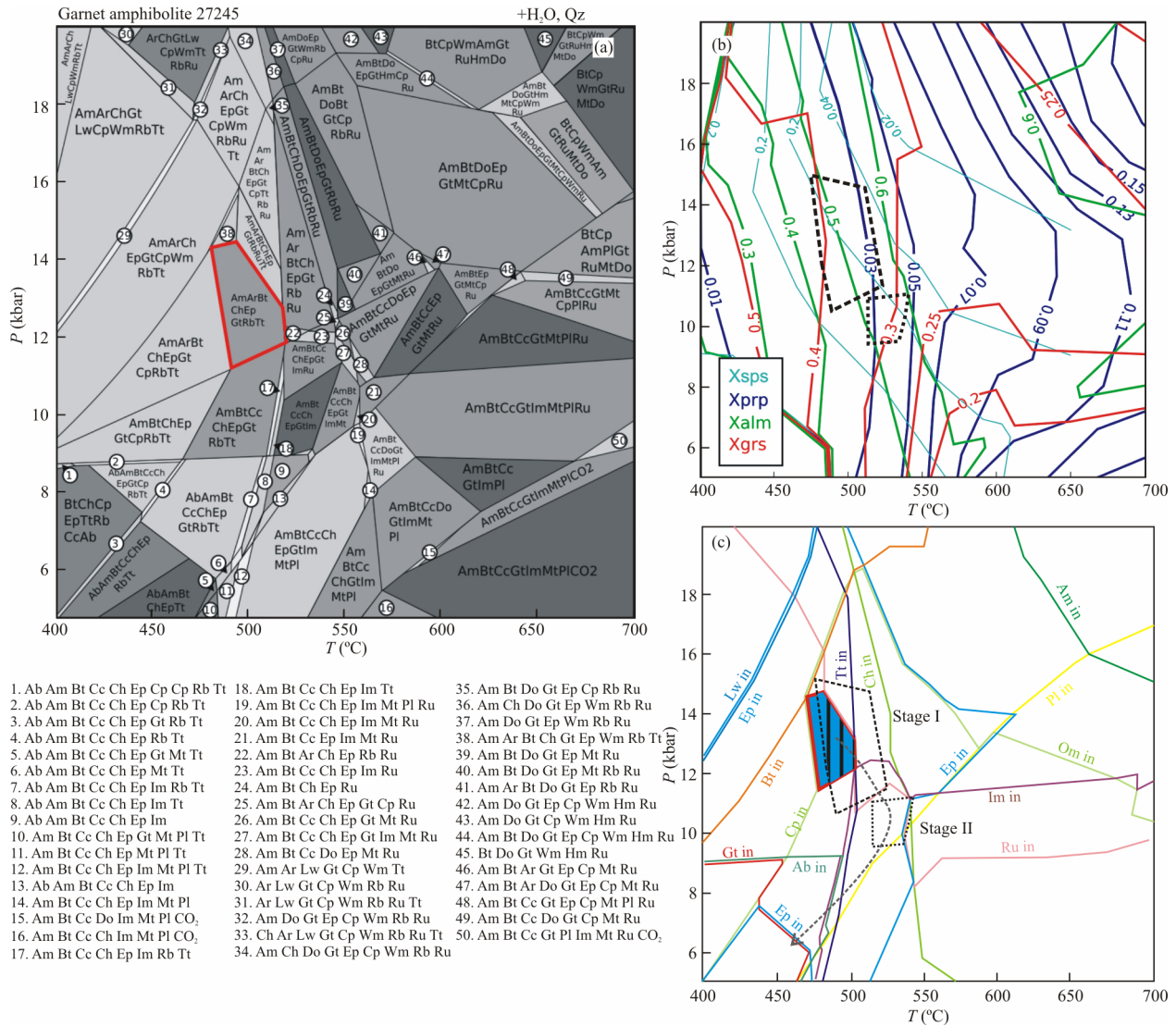


**Figure 9.** (a) *PT* pseudosection of garnet amphibolite sample 27245 in the system SiO<sub>2</sub>-TiO<sub>2</sub>-Al<sub>2</sub>O<sub>3</sub>-FeO-MgO-MnO-CaO-Na<sub>2</sub>O-K<sub>2</sub>O-H<sub>2</sub>O-CO<sub>2</sub>-O<sub>2</sub>. Shading of *PT* fields as in Fig. 8. The field of the observed peak metamorphic assemblage is marked in red. (b) Isoleths of garnet end member fractions. The stippled field marks the optimal convergence for the garnet core compositions, the dotted field for the rim compositions. (c) *PT* fields of single mineral phases. *PT*-path defined by stage I (vertically ruled field) with the overlap of garnet core compositions with the field of the observed assemblage, stage II by the field of garnet rim compositions and finally by fields of retrograde assemblages.

limits of the *PT*-fields of rutile, biotite and epidote as well as the upper temperature limits of the *PT* fields of lawsonite and chlorite. Ilmenite which is well represented in the natural assemblage only appears in the *PT* pseudosection in *PT* fields at slightly lower pressure.

The isopleths of the garnet end-member molar fractions for the garnet core only show a weak convergence in this *PT* pseudosection. As a result, minima and maxima of the core analyses overlap in a wide field (Fig. 9b). However, the overlap of this field with the *PT* field of the observed peak metamorphic assemblage restricts the peak pressure conditions at 11.7–14.5 kbar, 480–510 °C (stage I) for garnet amphibolite sample 27245. On the other hand, isopleths converge much better for the garnet rim compositions at 9.5–11.0 kbar, 535–560 °C. This field entirely overlaps with two assemblages realized in sample 27245: the first one is garnet-amphibole- biotite-chlorite-epidote-calcite-ilmenite, the second contains additional magnetite. Hence the *PT* condi-

tions of this field restrict the peak temperature conditions (stage II). The further retrograde *PT* path can be well confined by the *PT* field of albite <9 kbar, <500 °C, where the conspicuous late albite porphyroblasts of the rock grew, which enclosed all priorly formed mineral phases. The phenomenon is a well known feature occurring on the retrograde decompression path of metapelitic and metabasic high pressure rocks. Jamieson and O’Beirne-Ryan (1991) could show semiquantitatively calculating activity diagrams of fluid species that the stability field of albite would be enlarged during pressure and temperature decrease and hence further albite growth was triggered.

3.2.2.3 Granite gneiss (sample 27241)

The *PT* pseudosection calculated for the granite gneiss sample 27241 (Fig. 10a) shows that the dominant assemblage garnet-biotite-phengite-epidote-albite-K-feldspar-quartz-titanite-magnetite is a metamorphic assemblage occurring in a wide *PT*-field at

intermediate temperature and intermediate to high pressures around 5–16 kbar, 450–650 °C. The field is well bounded by the lower temperature limit of garnet and magnetite, the lower pressure limit of omphacite, which is also the upper pressure limit of albite and biotite, the lower pressure limit of epidote, which is also the upper pressure limit of plagioclase. Surprisingly, isopleths of the garnet end-member molar fractions for the garnet core converge in a very restricted *PT* field at high pressure and temperature at 15.6–17.0 kbar, 660–690 °C (Figs. 10b, 10c). This field merges into the *PT*-field of omphacite, which is not observed. Hence the overlap with the field of the observed assemblage restricts conditions for stage I to even 15.6–16.2 kbar, 660–675 °C. Isopleths for garnet rim composition converge in a narrow close *PT* field, at 15.0–15.6 kbar, 650–670 °C. Garnet obviously grew along a very short early cooling-decompression path that is subsequently followed towards low pressure and temperature within the wide field of the observed assemblage.

3.2.2.4 Garnet micaschist (sample 27250)

Calculation of a *PT* pseudosection for garnet micaschist sample 27250 (Fig. 11a) which occurs within the eclogite unit in close vicinity to an eclogite as well as a garnet amphibolite occurrence (Fig. 2b) yields relatively well defined *PT* fields for the

observed peak metamorphic assemblages garnet-chlorite-biotite-plagioclase-magnetite and with additional paragonite at 6.5–9.0 kbar, 565–610 °C. Paragonite was not observed, but could be present in small amounts. The *PT* field is well restricted to the close upper pressure limits of the *PT* fields of plagioclase and magnetite, lower pressure limit of the clinopyroxene field, lower temperature limit of the garnet and staurolite fields and upper temperature limit of the chlorite field (Fig. 11c). Also the isopleth of the maximum Ca-content of 0.24 apfu in the plagioclase occurs only slightly outside the field of the observed assemblage. However, isopleth of the maximum Si-content of 3.33 apfu in white mica occurs at much higher pressure near the *PT*-field of chloritoid above 17.5 kbar that was observed as inclusion in garnet. The isopleth of  $X_{Mg}$  of 0.25 in this chloritoid also plots close. The high-Si phengite and the chloritoid inclusions define higher pressure relicts (stage I). Isopleths of the garnet end-member molar fractions for core and rim converge in a rather wide field partly overlapping with the field of the observed assemblage (Fig. 11b). However, the isopleth of the maximum grossular content of 0.23 plots also near the relict phengite and chloritoid composition. Hence a field of 17–18.5 kbar, 475–525 °C would define an approximate location of a relict high pressure stage I. On the other hand, the overlap of the field of most garnet compositional isopleths with the observed

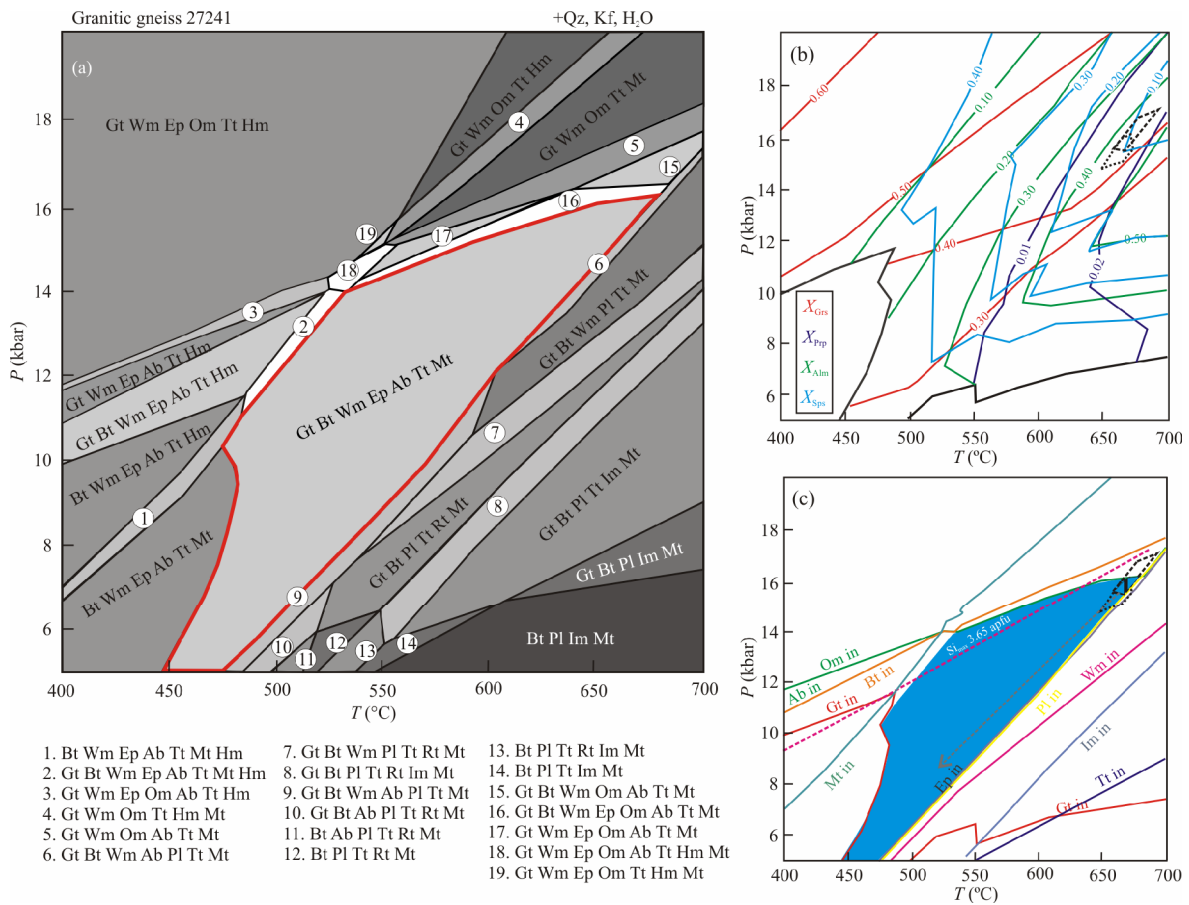


**Figure 10.** (a) *PT* pseudosection of granite gneiss sample 27241 in the system SiO<sub>2</sub>-TiO<sub>2</sub>-Al<sub>2</sub>O<sub>3</sub>-FeO-MgO-MnO-CaO-Na<sub>2</sub>O-K<sub>2</sub>O-H<sub>2</sub>O-O<sub>2</sub>. Shading of *PT* fields as in Fig. 8. The field of the observed peak metamorphic assemblage is marked in red. (b) Isopleths of garnet end member fractions. The stippled field marks the optimal convergence for the garnet core compositions, the dotted field for the rim compositions. (c) *PT* fields of single mineral phases. *PT*-path defined by stage I (vertically ruled field) with the overlap of garnet core compositions and the field of the observed assemblage, stage II by the field of garnet rim compositions and finally by fields of retrograde assemblages.

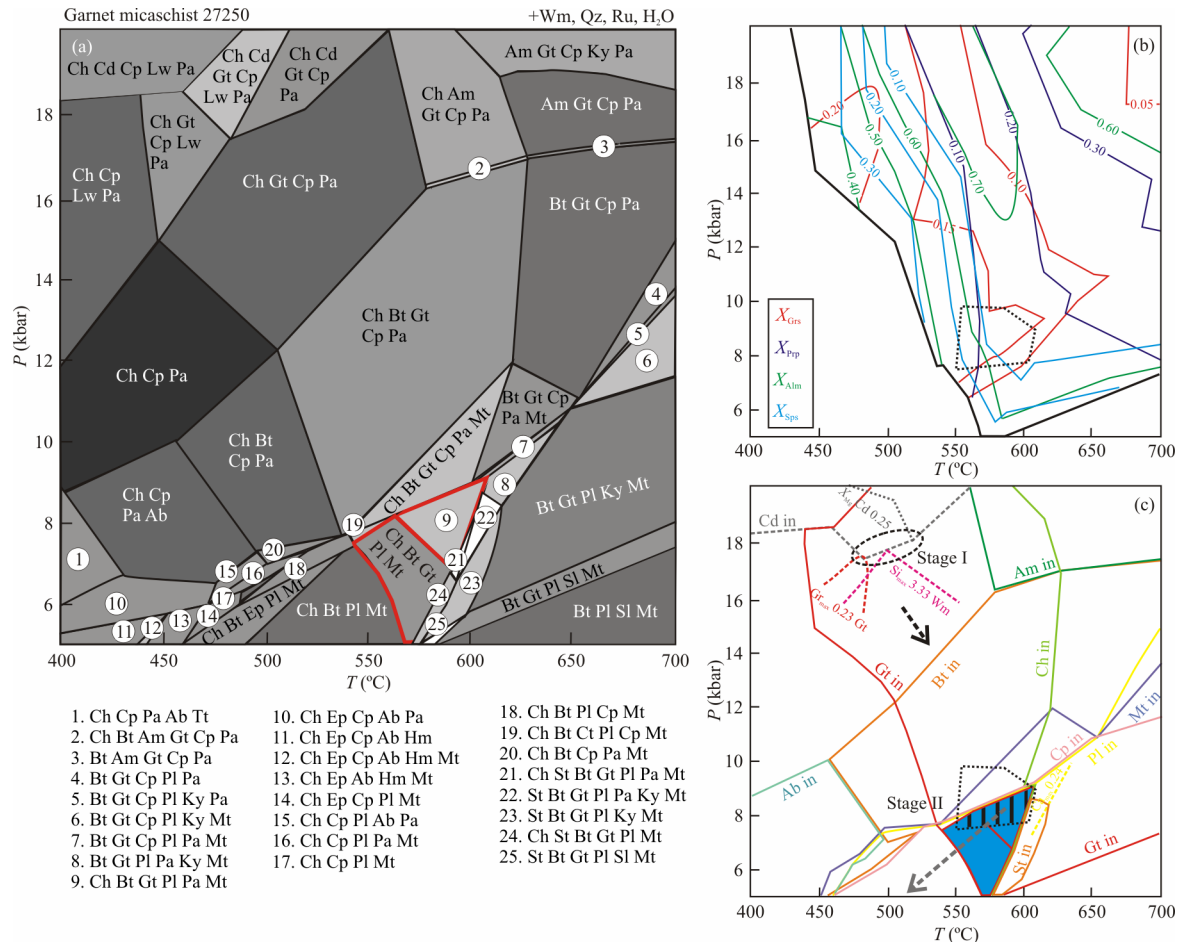


**Figure 11.** (a) *PT* pseudosection of garnet micaschist sample 27250 in the system  $\text{SiO}_2\text{-TiO}_2\text{-Al}_2\text{O}_3\text{-FeO-MgO-MnO-CaO-Na}_2\text{O-K}_2\text{O-H}_2\text{O-O}_2$ . Shading of *PT* fields as in Fig. 8. The field of the observed peak metamorphic assemblage is marked in red. (b) Isopleths of garnet end member fractions. The stippled field marks the optimal convergence for the garnet core and rim compositions. (c) *PT* fields of single mineral phases. Stage I is defined by few relict mineral compositions, stage II (vertically ruled field) with the overlap of garnet core and rim compositions and the field of the observed assemblage and by fields of retrograde assemblages.

assemblage can restrict the field for the formation of garnet during a later strong overprint at 7.5–9.0 kbar, 555–610 °C (stage II; Fig. 2c). The retrograde path occurred during decompression and cooling well within the *PT* field of plagioclase and confirms the late porphyroblastic growth of plagioclase mimetically across schistosity and crenulation hinges. The *PT* field of albite, which is not observed as matrix phase, occurs in the calculated *PT* pseudosection at  $\leq 9$  kbar,  $\leq 470$  °C.

### 3.3 Rb-Sr Geochronology

For eclogite sample 27231 we separated three grain size fractions of white mica, one apatite fraction and three omphacite fractions. Omphacite was separated into two density fractions ( $\rho > 3.26$ , corresponding to more Fe-rich omphacite, and  $\rho < 3.26$ , comparatively Fe-poor omphacite) and one fraction of particularly small grain size ( $< 160$   $\mu\text{m}$ ). All mineral fractions were meticulously purified; special care was taken to obtain amphibole-free omphacite separates. Deformed white mica oriented parallel to a joint plane in the sample was separated, purified and used as an additional fraction. Analytical data are given in Table 3. Seven fractions from the eclogite matrix (ex-

cept for the deformed white mica) define an isochron with a date of  $532.2 \pm 9.1$  Ma (MSWD=7.1, Fig. 12). The elevated MSWD of 7.1 is due to very minor Sr-isotopic disequilibria between apatite and the omphacite fractions. The reason for the disequilibria remains unclear; however, this does not affect the slope of the regression line, and exclusion of either apatite or omphacite fractions does not change the resulting age information to any significant extent. It is notable that no correlation exists between grain size and apparent age for the white mica fractions in the eclogite matrix. This indicates that no relict grains from earlier metamorphic stages are present, that the formation of the dated assemblage was a short-term process (cf., Angiboust et al., 2014), the duration of which is covered by the uncertainty of the calculated Rb-Sr date. Hence we interpret the 7-point-isochron date as the age of crystallisation of the here analyzed peak metamorphic eclogite assemblage. Formation of narrow, lower-Si white mica rims during retrograde metamorphism and also the formation of the compositional range of omphacite must have occurred within the time range given by the uncertainties of the age.

The additional fraction of deformed white mica plots below

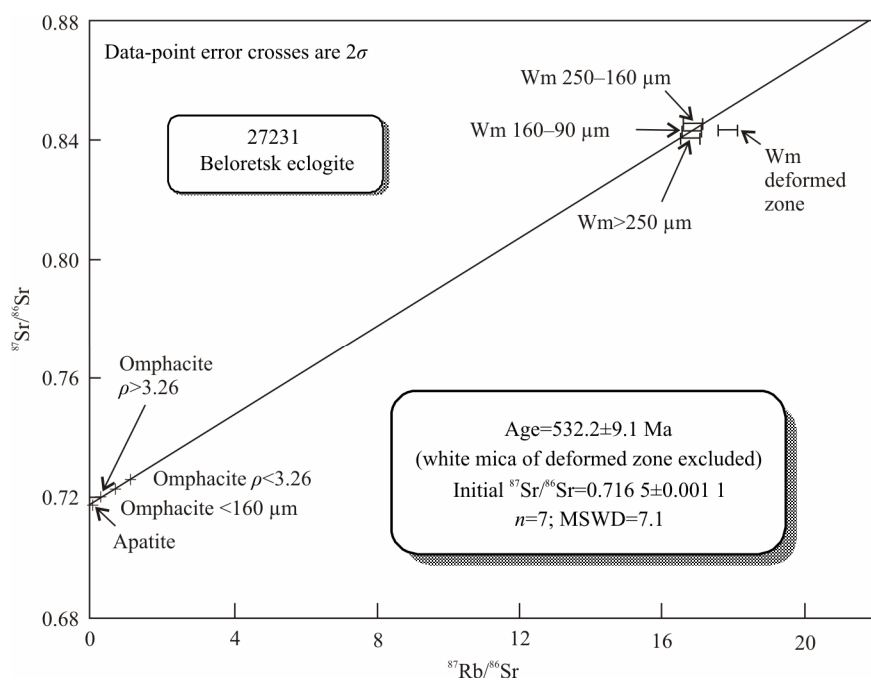


**Figure 12.** Seven-point Rb/Sr mineral isochron of the eclogite assemblage in sample 27231 defined by grain size fractions of white mica of phengite composition, grain size and density fractions of omphacite and an apatite fraction. An additional fraction of deformed white mica points to a younger age.

**Table 3** Rb/Sr isotope data of mineral fractions in eclogite sample 27231

Sample No.	Material	Rb (ppm)	Sr (ppm)	$^{87}\text{Rb}/^{86}\text{Sr}$	$^{87}\text{Sr}/^{86}\text{Sr}$	$^{87}\text{Sr}/^{86}\text{Sr } 2\sigma_m$
PS3243	White mica 250–160 $\mu\text{m}$	541	94.2	16.9	0.844 324	0.002 0
PS3244	White mica >250 $\mu\text{m}$	487	84.7	16.8	0.839 937	0.001 9
PS3245	White mica 160–90 $\mu\text{m}$	477	83.1	16.8	0.841 782	0.002 4
PS3246	Apatite	0.205	261	0.002 27	0.716 413	0.004 4
PS3247	Omphacite $\rho>3.26$	4.32	41.3	0.303	0.718 817	0.002 1
PS3248	Omphacite <160 $\mu\text{m}$	9.96	45.2	0.639	0.721 296	0.003 2
PS3250	Omphacite $\rho<3.26$	17.7	45.3	1.13	0.724 904	0.002 8
PS3249	White mica in vein	483	79.4	17.8	0.842 460	0.001 4

the isochron and points to a younger age of formation of this texturally peculiar white mica. An apatite-white mica isochron would formally yield an age of  $504\pm 7$  Ma. No clear assignment of this weakly defined age to a specific event can be given. This age only indicates that a weak late- to post-Timanian overprint affected that particular sample.

## 4 DISCUSSION

### 4.1 Interrelated Pressure-Temperature Paths

We included all *PT*-data for garnet core and rim compositions extracted from the four pseudosection calculations (Figs. 8, 9, 10, 11) and the derived *PT* paths into Fig. 13 to show relationships between the different *PT*-evolutions of the rocks studied. It is notable that peak pressures decrease from the lower to the upper units of the BMC as predicted by the distribution of metamorphic facies assemblages (Fig. 2c). *PT*-paths of eclogite and garnet amphibolite show classical clockwise interrelated loops which are significantly different in pressures and temperatures. They start at a low metamorphic gradient of around  $10^\circ\text{C}/\text{km}$  at peak pressure conditions with nucleation of garnet (stage I) followed by an early

heating-decompression trajectory towards peak temperature conditions (stage II) where garnet growth ends along a higher metamorphic gradient of around  $15^\circ\text{C}/\text{km}$ . This is followed by decompression-cooling trajectories which converge at low pressure and temperature. This classic loop pattern is well known from collision wedges at the interface between colliding continental plates (e.g., Spear, 1993). However, the further two studied felsic samples from the eclogite unit show strongly deviating patterns. The Achmerovo granite gneiss, which has the same Mesoproterozoic protolith age as the eclogite of around 1 350 Ma (Krasnobayev et al., 2008; Glasmacher et al., 2001), was also overprinted at a similar high pressure as the eclogite confirming an “*in situ*” origin of the eclogite. However, peak metamorphic temperatures were about  $150^\circ\text{C}$  higher than for the eclogite. This could be explained by subduction of the granite gneiss in the outermost part of a collisional wedge against a still hot upper plate being cooled by subsequent underplating of cool crust during concomitant exhumation. The *PT* path of the granite gneiss converges with the trajectory of the eclogite at intermediate crustal levels. The garnet micaschist shows few compositional relicts of a possible high



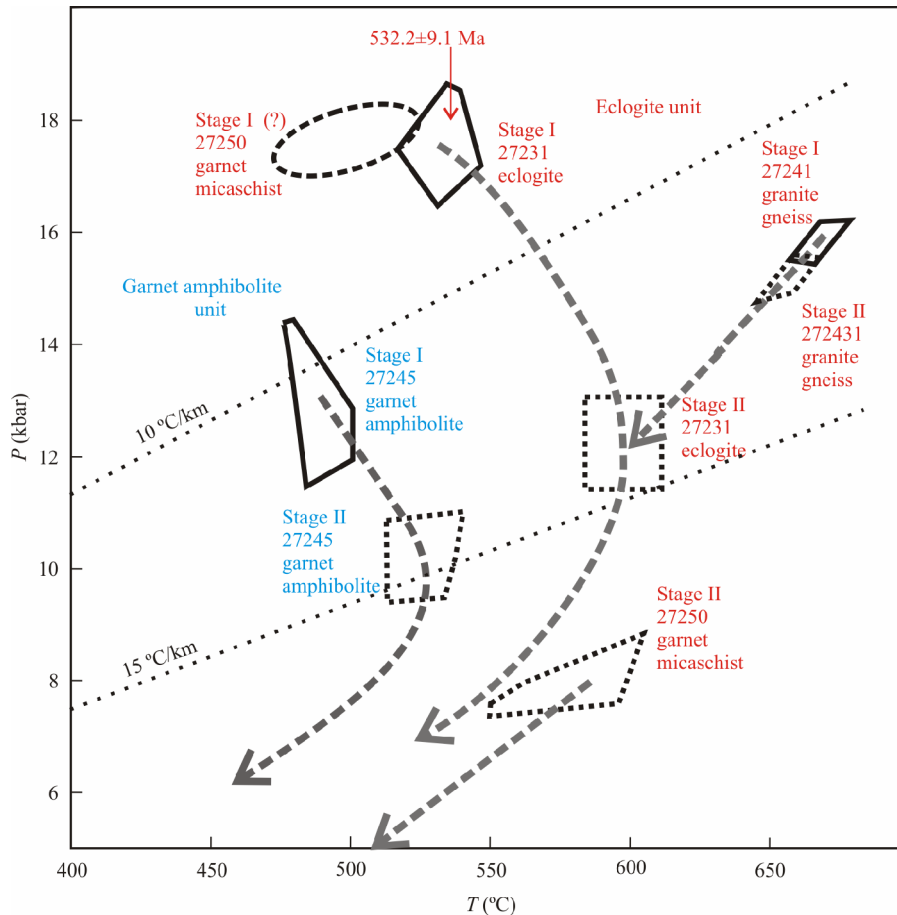


Figure 13. Interrelated  $PT$  paths of rocks from the structurally lowermost units of the BMC as derived in Figs. 8, 9, 10 and 11.

pressure stage I near the one of eclogite, but mostly conserved peak temperature conditions of 7.5–9.0 kbar, 555–610 °C close to the late  $PT$  path of the eclogite. In this case we suggest almost complete recrystallisation of the metamorphic assemblage at intermediate crustal levels during a deformation event and influx of external fluids causing dissolution and reprecipitation of phases.

The Rb/Sr mineral isochron age of 532.2±9.1 Ma dates the crystallisation of the peak metamorphic assemblage during the Early Cambrian, suggesting that the whole set of interrelated  $PT$  paths originated close to that age during exhumation of the BMC. Currently we only know that exhumation ends before ~490 Ma considering the age of the unconformity below the Lower Ordovician cover on the BMC (Puchkov, 2013). For the eclogite it would mean that exhumation from an original depth of 62 km (calculated with a mean crustal density of 2.8 g/cm<sup>3</sup>) occurred within 42 Ma resulting in a minimum moderate exhumation rate of ~1.5 mm/a. This would be an order of magnitude higher than general mean erosion rates of 0.05 mm/yr and rates of 0.2–0.8 mm/a for erosion-controlled exhumation of accretionary wedges in California and Chile (Willner et al., 2005; Ring and Brandon, 1999). A moderate exhumation rate was proposed by Hetzel and Romer (2000) for early exhumation in the Devonian collisional wedge of the Urals. A similar geotectonic environment for the BMC is conceivable. The present thickness of the crustal pile of the BMC, which is tilted towards the NNW, is by far less than the original crustal thickness above the eclogite unit. The same applies to the originally ~14 km original difference of depth be-

tween the eclogite and garnet amphibolite. This means that crust must have been excised during exhumation of the BMC and units rather represent nappes. Most likely normal faulting at the top of a collisional wedge during forced return flow was responsible for excision of a considerable amount of crust during exhumation as predicted from a collisional wedge model by Ring and Glodny (2010).

#### 4.2 Timing of Timanide Orogenic Events

The Rb/Sr mineral isochron age of 532.2±9.1 Ma of the peak metamorphic conditions of the Beloretsk eclogite has important implications for the timing of Timanide metamorphism in the SW Urals in general. The age is comparable to white mica <sup>40</sup>Ar/<sup>39</sup>Ar plateau ages of 543±3 and 550±4 Ma in metapelitic rocks of the BMC eclogite unit and of 541±3 and 543±4 Ma within the lower part of the BMC garnet amphibolite unit (Glasmacher et al., 2001; Fig. 2a). Contrasting to Glasmacher et al. (2001) we interpret these <sup>40</sup>Ar/<sup>39</sup>Ar plateau ages as ages of crystallisation of the metamorphic white mica, although the metamorphic temperatures estimated for BMC samples by far exceed those of the frequently cited range of white-mica <sup>40</sup>Ar/<sup>39</sup>Ar closure temperatures of ~350–420 °C (McDougall and Harrison, 1999 and references therein). Villa (2015, 2006, 1998 and references therein) has widely pointed out that strain and fluid availability are commonly more important in isotope redistribution for the <sup>40</sup>Ar/<sup>39</sup>Ar system at medium and high metamorphic grade and hence that many estimates of its closure temperature are too low. Already Wi-

jbans and McDougall (1986) suggested that age reset by volume diffusion will only occur when other faster processes are absent or unimportant. We thus do not consider volume diffusion to be important for any of the dated samples in the BMC, and conclude that the consistent Rb-Sr and Ar-Ar white mica-based ages between ~530 and ~550 Ma date white mica crystallization or the last episode of dynamic recrystallization of white mica, with absence of major post-530 Ma deformation or fluid driven overprints. This also implies that all three ductile deformation events within the BMC as described by Glasmacher et al. (2001) are invariably of Timanide age.

However, two  $^{40}\text{Ar}/^{39}\text{Ar}$  white mica plateau ages of  $557\pm 4$  and  $597\pm 4$  Ma in the upper part of the BMC garnet amphibolite unit (Glasmacher et al., 2001; Fig. 2a) are significantly older than the Rb/Sr isochron age and the  $^{40}\text{Ar}/^{39}\text{Ar}$  white mica ages in the eclogite unit. Also  $^{40}\text{Ar}/^{39}\text{Ar}$  spot ages of detrital phengite in Upper Vendian sedimentary rocks derived from the eroding upper part of BMC yielded older values in the range of 571–609 Ma (Willner et al., 2004:  $571\pm 52$ ,  $585\pm 32$ ,  $594\pm 41$ ,  $609\pm 6$  Ma). Hence a trend of increasing ages from bottom to top of the BMC appears likely. This concurs with a decrease of peak metamorphic pressures of the units in the same direction. This phenomenon could be explained by successive underthrusting in the BMC with the youngest underplated material in the SSE.

Crystallisation ages identical to the age of the Beloretsk eclogite were derived by Rb/Sr mineral isochron dating of blueschists at  $535\pm 6$ ,  $536\pm 7$ ,  $536\pm 19$  Ma in the Kvarqush anticlinorium ~600 km further north (Beckholmen and Glodny, 2004; Fig. 1, Fig. 14a). These ages date peak blueschist facies conditions of 7–8 kbar/350–400 °C (Rusin, 1996) proving comparable conditions along strike of the ancient convergent margin. This is also valid, when the three ages derived by Beckholmen and Glodny (2004) are recalculated with the new  $^{87}\text{Rb}$  decay constant used in this work ( $544\pm 6$ ;  $545\pm 7$ ;  $545\pm 19$  Ma). In the Kvarqush anticlinorium an extensive unit comprising metapelitic and metabasic rock with blueschist, greenschist, and subgreenschist facies overprint occur in the immediate footwall of the Main Uralian fault, i.e., the easternmost exposed pre-Uralian margin. This complex likely represents a typical accretionary prism at a convergent margin (e.g., Willner, 2005). Its Early Cambrian age of metamorphism is also within the range of widespread earlier derived K/Ar ages of white mica at 503–552 Ma (Nikiforov and Kaleganov, 1991).

Kuznetsov et al. (2010, 2007) summarized the full extent of the pre-Uralide (Timanide) orogeny providing an uncovered map including information from outcrop and drill cores (Fig. 14a). Particularly they showed the distribution of Neoproterozoic to Middle Cambrian intrusions and evaluated their geodynamic setting. The western Timanides contain calc-alkaline Ediacaran–Middle Cambrian intrusions into mainly sedimentary units with provenance of detritus from Baltica and are thus interpreted as the former convergent eastern pre-Uralide margin of Baltica. The northeastern branch of the Timanides (north of 60°N) contain widespread Ediacaran–Middle Cambrian volcanosedimentary series and intrusions that represent calc-alkaline as well as younger A-type series. This branch is thought to be part of a continent called Arctida with a tentative Ediacaran suture zone against the E-margin of Baltica. In this setting the

Beloretsk eclogite and the Kvarqush blueschist confirm existence of a long Ediacaran–Early Cambrian convergent margin at the eastern periphery of Baltica. Also Shardakova (2016) confirmed calcalkaline magmatism in the range 510–660 Ma for the Bashkirian mega-anticlinorium and the adjacent Ufaley Block in NW. It is also notable that  $^{40}\text{Ar}/^{39}\text{Ar}$  spot ages of detrital magmatic muscovite in Upper Vendian sedimentary rocks derived from the eroding Timanide arc yielded values in the range of 645–732 Ma (Willner et al., 2004).

### 4.3 Geodynamic Implications

Whereas the geodynamic environment for the unit containing the Kvarqush blueschist at the outer pre-Uralide margin can be classified as accretionary prism, a geodynamic assignment for the Beloretsk Complex is not evident. Although the BMC originated along an overall convergent margin, its position is rather to the west of the Timanide magmatic arc (Fig. 14a). Moreover, the protoliths of the BMC were shelf sediments and were intruded by Mesoproterozoic bimodal dykes. These point to a HP overprint within a collisional wedge rather than within a subduction channel below accretionary prisms at convergent margins, because subduction channel rocks would rather consist of oceanic metasediments, metagreywackes, serpentinites and metabasites of oceanic origin (e.g., Meyer et al., 2014; Willner, 2005 and references therein). As alternative, a closure of a small back-arc oceanic seaway could be envisaged that might have opened already during the Mesoproterozoic Mashak event (Puchkov et al., 2013). However, in spite of the fact that the BMC represents Baltican crust, the BMC might have been emplaced by transcurrent movement along the convergent margin. For instance, during the second deformation phase described by Glasmacher et al. (2001) sinistral transtensional shear zones originated within the BMC that might be structures of emplacement of the BMC. Even the Zuratkul fault that separates the remarkably different tectono-metamorphic regimes could represent a late transcurrent emplacement structure. Willner et al. (2001) had proposed such transcurrent emplacement comparing the setting for the BMC with the wide spread displacement of HP rocks in the Caribbean along major transcurrent faults during the change of the passive northern margin of South America to an active one in the Late Mesozoic (Pindell and Barrett, 1990). Nevertheless, it has to be born in mind that a lot of information on the Timanide margin in the SW Urals is unknown, i.e., it might be incorporated as relicts in the Devonian metamorphic complexes west of the Main Uralian fault or even to the east of it under the Magnitogorsk arc (see Fig. 1).

Following earlier paleocontinental reconstructions (e.g., Willner et al., 2014; Nance et al., 2012; Torsvik et al., 1996; Nance and Murphy, 1994; Fig. 14b), the Timanide convergent margin most likely continued into the Avalonian and Cadomian/Armorican convergent margin along the periphery of the western Gondwana around the time when the former Rodinia supercontinent broke off. Also this remarkable convergent margin that is comparable in length with the present one on the Pacific margin of both Americas was mainly reconstructed by the occurrence of Neoproterozoic–Cambrian calc-alkaline magmas. It is astonishing that in the Avalonian part only one occurrence of Neoproterozoic high pressure rocks

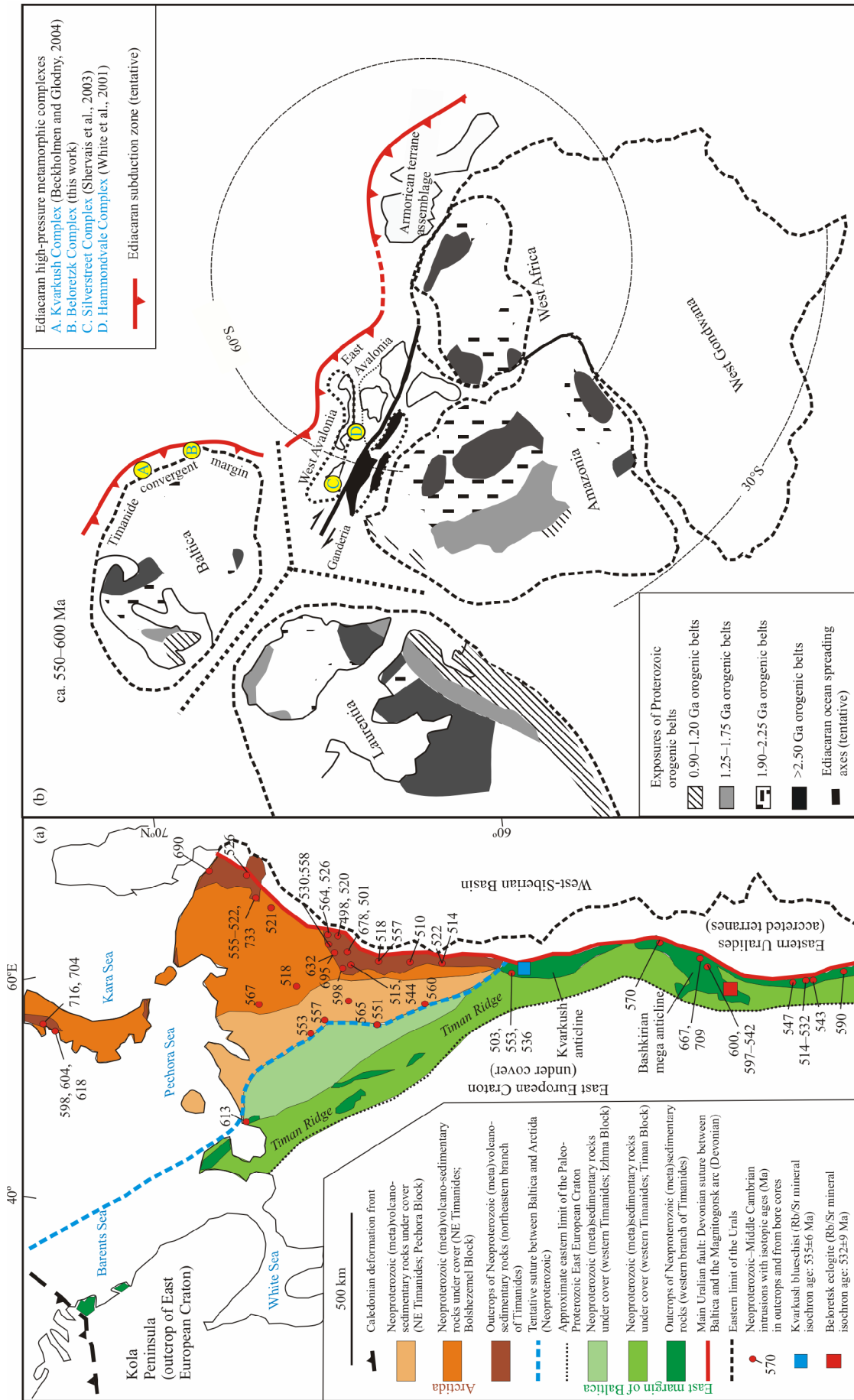


**Figure 14.** (a) Uncovered map of the pre-Uralides (Timanides) redrawn and simplified after Kuznetsov et al. (2010, 2007). Isotopic data collection and nomenclature follows Kuznetsov et al. (2010, 2007). (b) Paleogeographical map showing the postulated position of a coherent Timanide-Avalonian-Armorian convergent margin along West Gondwana at about 600–550 Ma, when Laurentia and Baltica just separated from West Gondwana following the break-up of Rodinia. Restoration modified after Willner et al. (2014) based on the paleocontinental reconstruction of Torsvik et al. (1996) and reconstructions by Nance et al. (2012), Nance and Murphy (1994). Locations of Neoproterozoic high-pressure rocks along the convergent margin are inserted.

is known at Hammondvale/New Brunswick (White et al., 2001) and existence of a likely Neoproterozoic eclogite is indirectly proposed for the Silverstreet eclogite in the Avalonian Carolina terrane in South Carolina by Shervais et al. (2003), but not yet confirmed by direct isotopic dating. However, no Neoproterozoic high pressure rocks are known as yet from the Armorican part of the long convergent margin. Hence there is a remarkable gap of knowledge to be filled in the future.

## 5 CONCLUSIONS

*PT* pseudosection techniques provide an excellent tool to study the *PT* evolution of “*in situ*” eclogite facies assemblages and the nature of transition to albite-epidote-amphibolite facies assemblages within a collisional wedge. Metabasic assemblages originated under water-saturated conditions at high pressures, which are mainly recorded by garnet and partly phengite core compositions. This stage is followed by characteristic decompression-heating paths during thermal relaxation to a second stage recorded by garnet rim compositions. The geometry of later decompression-cooling paths can be narrowed by effects of late metamorphic overprints. Felsic rocks in the eclogite unit partly preserve peak eclogite facies conditions: The granite gneiss was neither overprinted by deformation nor by fluid influx after attaining its high pressure overprint, whereas only high pressure relicts could be detected in the garnet micaschist which was strongly reequilibrated at midcrustal conditions due to localized penetrative deformation and related strong external fluid influx.

Our Rb/Sr mineral isochron age of the peak *PT* eclogite assemblage of  $532 \pm 9$  Ma can be shown to date a crystallisation and not a cooling event. It helps to reinterpret earlier

$^{40}\text{Ar}/^{39}\text{Ar}$  ages of phengite in metapelitic rocks in the BMC. In the BMC decreasing ages are correlated with increasing pressures indicating successive underplating within a collisional wedge. Closure of a back arc seaway and/or transcurrent emplacement of the HP rocks along a convergent margin is possible. Metamorphic ages of the BMC correlate with locally known HP rocks of an accretionary prism (Kvarkush blueschist) in 600 km distance along the Timanide convergent margin, which could be traced along the full length of the eastern periphery of Baltica due to widespread ages of Ediacaran to Mid-Cambrian magmatism.

## ACKNOWLEDGMENTS

This publication is dedicated to the memory of Aleksey A. Alekseev who guided the first author to the Beloretsk Complex in 1999 and shared his knowledge with him. He sadly passed away in 2008. Samples were collected during a field leg in 1999 that was financed by Deutsche Forschungsgemeinschaft (No. Wi 875-6/1, 2) to Arne P. Willner, which is gratefully acknowledged. We thank R. Klemd and S. Sindern for their helpful suggestions. The final publication is available at Springer via <https://doi.org/10.1007/s12583-019-1249-2>.

**Electronic Supplementary Materials:** Supplementary materials (ESM1 and ESM2) are available in the online version of this article at <https://doi.org/10.1007/s12583-019-1249-2>.

## REFERENCES CITED

- Alekseev, A. A., 1984. Riphean and Vendian Magmatism in the Southern Urals. Nauka, Moscow. 136 (in Russian)
- Alekseev, A. A., Alekseeva, G. V., Galieva, A. R., et al., 2006. Metamorphic Geology of the Western Slope of the Southern Urals. Gilem, Ufa. 212 (in Russian)
- Alekseev, A. A., Kovalev, S. G., Timofeeva, Y. A., 2009. The Beloretsk Metamorphic Complex. Dizain Poligraph Service, Ufa. 208 (in Russian)
- Angiboust, S., Glodny, J., Oncken, O., et al., 2014. In Search of Transient Subduction Interfaces in the Dent Blanche-Sesia Tectonic System (W. Alps). *Lithos*, 205: 298–321. <https://doi.org/10.1016/j.lithos.2014.07.001>
- Beckholmen, M., Glodny, J., 2004. Timanian Blueschist-Facies Metamorphism in the Kvarkush Metamorphic Basement, Northern Urals, Russia. *Geological Society, London, Memoirs*, 30(1): 125–134. <https://doi.org/10.1144/gsl.mem.2004.030.01.11>
- Berman, R. G., 1988. Internally-Consistent Thermodynamic Data for Minerals in the System  $\text{Na}_2\text{O}-\text{K}_2\text{O}-\text{CaO}-\text{MgO}-\text{FeO}-\text{Fe}_2\text{O}_3-\text{Al}_2\text{O}_3-\text{SiO}_2-\text{TiO}_2-\text{H}_2\text{O}-\text{CO}_2$ . *Journal of Petrology*, 29(2): 445–522. <https://doi.org/10.1093/ptrology/29.2.445>
- Berman, R. G., 1991. Thermobarometry Using Multi-Equilibrium Calculations: A New Technique, with Petrological Applications. *Canadian Mineralogist*, 29: 833–855
- Bernhardt, H.-J., 2010. MINCALC-V5, a non EXCEL Based Computer Program for General Electron-Microprobe Mineral Analyses Data Processing. Abstract of 20th IMA-Meeting, Session XO150G. 869
- Brown, D., Juhlin, C., Alvarez-Marron, J., et al., 1998. Crustal-Scale Structure and Evolution of an Arc-Continent Collision Zone in the Southern Urals, Russia. *Tectonics*, 17(2): 158–170. <https://doi.org/10.1029/98tc00129>
- Brown, D., Spadea, P., Puchkov, V., et al., 2006. Arc Continent Collision in the Southern Urals. *Earth Science Reviews*, 79: 261–287
- Cohen, K. M., Finney, S. C., Gibbard, P. L., et al., 2013. The ICS International Chronostratigraphic Chart. *Episodes*, 36(3): 199–204. <https://doi.org/10.18814/epiiugs/2013/v36i3/002>
- Connolly, J. A. D., 1990. Multivariable Phase Diagrams: An Algorithm Based on Generalized Thermodynamics. *American Journal of Science*, 290(6): 666–718. <https://doi.org/10.2475/ajs.290.6.666>
- Connolly, J. A. D., 2005. Computation of Phase Equilibria by Linear Programming: A Tool for Geodynamic Modeling and Its Application to Subduction Zone Decarbonation. *Earth and Planetary Science Letters*, 236(1/2): 524–541. <https://doi.org/10.1016/j.epsl.2005.04.033>
- Diener, J. F. A., Powell, R., White, R. W., et al., 2007. A New Thermodynamic Model for Clino- and Orthoamphiboles in the System  $\text{Na}_2\text{O}-\text{CaO}-\text{FeO}-\text{MgO}-\text{Al}_2\text{O}_3-\text{SiO}_2-\text{H}_2\text{O}-\text{O}_2$ . *Journal of Metamorphic Geology*, 25(6): 631–656. <https://doi.org/10.1111/j.1525-1314.2007.00720.x>
- Evans, B. W., 1990. Phase Relations of Epidote-Blueschists. *Lithos*, 25(1/2/3): 3–23. [https://doi.org/10.1016/0024-4937\(90\)90003-j](https://doi.org/10.1016/0024-4937(90)90003-j)
- Galieva, A. R., 2004. Geology, Petrology and Conditions of Origin of Eclogites and Host Rocks of the Beloretsk Metamorphic Complex (Southern Urals): [Dissertation]. Russian Academy of Science, Ufa. 144 (in Russian)
- Giese, U., Glasmacher, U. A., Kozlov, V., et al., 1999. Structural Framework of the Bashkirian Anticlinorium, SW Urals. *Geologische Rundschau*, 87(4): 526–544. <https://doi.org/10.1007/s005310050229>
- Glasmacher, U. A., Bauer, W., Giese, U., et al., 2001. The Metamorphic Complex of Beloretsk, SW Urals, Russia—A Terrane with a Polyphase Mesoproterozoic Thermo-Dynamic Evolution. *Precambrian Research*,



- 110(1/2/3/4): 185–213. [https://doi.org/10.1016/s0301-9268\(01\)00187-5](https://doi.org/10.1016/s0301-9268(01)00187-5)
- Glodny, J., Ring, U., Kühn, A., 2008. Coeval High-Pressure Metamorphism, Thrusting, Strike-Slip, and Extensional Shearing in the Tauern Window, Eastern Alps. *Tectonics*, 27(4): TC4004. <https://doi.org/10.1029/2007tc002193>
- Grazhdankin, D. V., Marusin, V. V., Meert, J., et al., 2011. Kotlin Regional Stage in the South Urals. *Doklady Earth Sciences*, 440(1): 1222–1226. <https://doi.org/10.1134/s1028334x11090170>
- Harris, M. A., 1977. The Stages of Magmatism and Metamorphism in the Pre-Jurassic History of the Urals and Preurals. Nauka, Moscow. 296 (in Russian)
- Hawthorne, F. C., Oberti, R., Harlow, G. E., et al., 2012. Nomenclature of the Amphibole Supergroup. *American Mineralogist*, 97(11/12): 2031–2048. <https://doi.org/10.2138/am.2012.4276>
- Hetzl, R., Romer, R. L., 2000. A Moderate Exhumation Rate for the High-Pressure Maksyutov Complex, Southern Urals, Russia. *Geological Journal*, 35(3/4): 327–344. <https://doi.org/10.1002/gj.862>
- Holland, T. J. B., Powell, R., 1998. An Internally Consistent Thermodynamic Data Set for Phases of Petrological Interest. *Journal of Metamorphic Geology*, 16(3): 309–343. <https://doi.org/10.1111/j.1525-1314.1998.00140.x>
- Holland, T. J. B., Powell, R., 1996. Thermodynamics of Order-Disorder in Minerals; II, Symmetric Formalism Applied to Solid Solutions. *American Mineralogist*, 81(11/12): 1425–1437. <https://doi.org/10.2138/am-1996-11-1215>
- Holland, T. J. B., Powell, R., 2003. Activity-Composition Relations for Phases in Petrological Calculations: An Asymmetric Multicomponent Formulation. *Contributions to Mineralogy and Petrology*, 145(4): 492–501. <https://doi.org/10.1007/s00410-003-0464-z>
- Jamieson, R. A., O’Beirne-Ryan, A. M., 1991. Decompression-Induced Growth of Albite Porphyroblasts, Fleur de Lys Supergroup, Western Newfoundland. *Journal of Metamorphic Geology*, 9(4): 433–439. <https://doi.org/10.1111/j.1525-1314.1991.tb00537.x>
- Kolesnikov, A. V., Marusin, V. V., Nagovitsin, K. E., et al., 2015. Ediacaran Biota in the Aftermath of the Kotlinian Crisis: Asha Group of the South Urals. *Precambrian Research*, 263: 59–78. <https://doi.org/10.1016/j.precamres.2015.03.011>
- Krasnobae, A. A., Kozlov, V. I., Puchkov, V. N., et al., 2008. The Akhmerovo Granite Massif: A Proxy of Mesoproterozoic Intrusive Magmatism in the Southern Urals. *Doklady Earth Sciences*, 418(1): 103–108. <https://doi.org/10.1134/s1028334x08010236>
- Krogh Ravn, E., 2000. The Garnet-Clinopyroxene Fe<sup>2+</sup>-Mg Geothermometer: An Updated Calibration. *Journal of Metamorphic Geology*, 18(2): 211–219. <https://doi.org/10.1046/j.1525-1314.2000.00247.x>
- Kuznetsov, N. B., Natapov, L. M., Belousova, E. A., et al., 2010. Geochronological, Geochemical and Isotopic Study of Detrital Zircon Suites from Late Neoproterozoic Clastic Strata along the NE Margin of the East European Craton: Implications for Plate Tectonic Models. *Gondwana Research*, 17(2/3): 583–601. <https://doi.org/10.1016/j.gr.2009.08.005>
- Kuznetsov, N. B., Soboleva, A. A., Udoratina, O. V., et al., 2007. Pre-Ordovician Tectonic Evolution and Volcano Plutonic Associations of the Timanides and Northern Pre-Uralides, Northeast Part of the East European Craton. *Gondwana Research*, 12(3): 305–323. <https://doi.org/10.1016/j.gr.2006.10.021>
- Leake, B. E., Woolley, A. R., Arps, C. E. S., et al., 1997. Nomenclature of Amphiboles Report of the Subcommittee on Amphiboles of the International Mineralogical Association Commission on New Minerals and Mineral Names. *European Journal of Mineralogy*, 9(3): 623–651. <https://doi.org/10.1127/ejm/9/3/0623>
- Lennykh, V. I., 1968. The Regional Metamorphism of the Precambrian Deposits of the Western Urals Western Slope and Ural-Tau Ridge. Uralian Branch of the USSR Academy of Science, Sverdlovsk. 67
- Ludwig, K., 2009. Isoplot V. 3.71: A Geochronological Toolkit for Microsoft Excel. Berkeley Geochronology Center, Berkeley, California. *Special Publication*, 4: 70
- Maslov, A. V., Erdtmann, B. D., Ivanov, K. S., et al., 1997. The Main Tectonic Events, Depositional History, and the Palaeogeography of the Southern Urals during the Riphean-Early Palaeozoic. *Tectonophysics*, 276(1/2/3/4): 313–335. [https://doi.org/10.1016/s0040-1951\(97\)00064-4](https://doi.org/10.1016/s0040-1951(97)00064-4)
- Matenaar, I., Glasmacher, U. A., Pickel, W., et al., 1999. Incipient Metamorphism between Ufa and Beloretzk, Western Fold-And-Thrust Belt, Southern Urals, Russia. *Geologische Rundschau*, 87(4): 545–560. <https://doi.org/10.1007/s005310050230>
- Matte, P., Maluski, H., Caby, R., et al., 1993. Geodynamic Model and <sup>39</sup>Ar/<sup>40</sup>Ar Dating for the Generation and Emplacement of the High Pressure (HP) Metamorphic Rocks in SW Urals. *Compte Rendu Academie de Science Paris*, 317: 1667–1674
- McDougall, I., Harrison, T. M., 1999. Geochronology and Thermochronology by the <sup>40</sup>Ar/<sup>39</sup>Ar Method. Oxford University Press, Oxford. 269
- Meyer, M., Klemm, R., Hegner, E., et al., 2014. Subduction and Exhumation Mechanisms of Ultra-High and High-Pressure Oceanic and Continental Crust at Makbal (Tianshan, Kazakhstan and Kyrgyzstan). *Journal of Metamorphic Geology*, 32(8): 861–884. <https://doi.org/10.1111/jmg.12097>
- Nance, R. D., Gutiérrez-Alonso, G., Keppie, J. D., et al., 2012. A Brief History of the Rheic Ocean. *Geoscience Frontiers*, 3(2): 125–135. <https://doi.org/10.1016/j.gsf.2011.11.008>
- Nance, R. D., Murphy, J. B., 1994. Contrasting Basement Isotopic Signatures and the Palinspastic Restoration of Peripheral Orogens: Example from the Neoproterozoic Avalonian-Cadomian Belt. *Geology*, 22(7): 617. [https://doi.org/10.1130/0091-7613\(1994\)022<0617:cbisat>2.3.co;2](https://doi.org/10.1130/0091-7613(1994)022<0617:cbisat>2.3.co;2)
- Nikiforov, O. V., Kaganov, B. A., 1991. Potassium-Argon Dating in the Zonal Metamorphism of the Kvarqush Plateau. *Ezhegodnik 1990, IGG Ekaterinburg, UrO AN SSSR*. 78–79 (in Russian)
- Pindell, J. L., Barrett, S. F., 1990. Geological Evolution of the Caribbean Region: A Plate-Tectonic Perspective. In: Dengo, G., Case, J. E., eds., *The Caribbean Region*. In: *The Geology of North America*, Vol. H. Geological Society of America, Boulder. 405–432
- Powell, R., Holland, T. J. B., 1999. Relating Formulations of the Thermodynamics of Mineral Solid Solutions: Activity Modeling of Pyroxenes, Amphiboles, and Micas. *American Mineralogist*, 84(1/2): 1–14. <https://doi.org/10.2138/am-1999-1-201>
- Puchkov, V. N., 1997. Structure and Geodynamics of the Uralian Orogen. In: Burg, J. P., Ford, M., eds., *Orogeny through Time*. *Geological Society London, Special Publications*, 121: 201–236
- Puchkov, V. N., 2010. Geology of the Urals and Pre-Urals. Russian Academy of Science, Ufa Branch, Institute of Geology, Ufa. 280
- Puchkov, V. N., 2013. Structural Stages and Evolution of the Urals. *Mineralogy and Petrology*, 107(1): 3–37. <https://doi.org/10.1007/s00710-012-0263-1>
- Puchkov, V. N., Bogdanova, S. V., Ernst, R. E., et al., 2013. The ca. 1 380 Ma Mashak Igneous Event of the Southern Urals. *Lithos*, 174: 109–124. <https://doi.org/10.1016/j.lithos.2012.08.021>
- Puchkov, V. N., Krasnobae, A. A., Sergeeva, N. D., 2014. The New Data on Stratigraphy of the Riphean Stratotype in the Southern Urals, Russia. *Journal of Geoscience and Environment Protection*, 02(3): 108–116. <https://doi.org/10.4236/gep.2014.23015>
- Rieder, M., Cavazini, G., D’Yakonov, Y. S., et al., 1998. Nomenclature of the Micas. *Canadian Mineralogist*, 36: 905–912
- Ring, U., Brandon, M. T., 1999. Ductile Deformation and Mass Loss in the Franciscan Subduction Complex: Implications for Exhumation Processes

- in Accretionary Wedges. *Geological Society, London, Special Publications*, 154(1): 55–86. <https://doi.org/10.1144/gsl.sp.1999.154.01.03>
- Ring, U., Glodny, J., 2010. No Need for Lithospheric Extension for Exhuming (U)HP Rocks by Normal Faulting. *Journal of the Geological Society*, 167(2): 225–228. <https://doi.org/10.1144/0016-76492009-134>
- Rusin, A. I., 1996. Metamorphic Map of the Northern Part of the Kvarokush Uplift (Northern Urals). Ezhegodnik 1995, IGG Ekaterinburg, UrO RAN. 96–99 (in Russian)
- Semikhatov, M. A., Shurkin, K. A., Aksenov, E. M., et al., 1991. A New Stratigraphic Scale for the Precambrian of the USSR. *Izvestiya, Akademiya Nauk SSSR, Ser. Geol.*, 4: 3–13 (in Russian)
- Shardakova, G. Y., 2016. Geochemistry and Isotopic Ages of Granitoids of the Bashkirian Mega-Anticlinorium: Evidence for Several Pulses of Tectono-Magmatic Activity at the Junction Zone between the Uralian Orogen and East European Platform. *Geochemistry International*, 54(7): 594–608. <https://doi.org/10.1134/s0016702916070089>
- Shervais, J. W., Dennis, A. J., Mcgee, J. J., et al., 2003. Deep in the Heart of Dixie: Pre-Alleghanian Eclogite and HP Granulite Metamorphism in the Carolina Terrane, South Carolina, USA. *Journal of Metamorphic Geology*, 21(1): 65–80. <https://doi.org/10.1046/j.1525-1314.2003.00416.x>
- Shvetsov, P. N., 1980. Stratigraphy of the Beloretzk Complex, Southern Urals. *Sovjetskaya Geologiya*, 3: 43–55 (in Russian)
- Sobolev, D., Avtoneyev, S. V., Belkovskaya, T. Y., et al., 1968. Tectonic Map of the Urals on a Scale 1 : 1 000 000 with Explanatory Notes. *Ural-Geologiya Sverdlovsk* (in Russian)
- Spear, F. S., 1993. *Metamorphic Phase Equilibria and Pressure-Temperature-Time Paths*. Mineralogical Society of America Monograph, Washington DC. 799
- Torsvik, T., Smethurst, M., Meert, J., et al., 1996. Continental Break-up and Collision in the Neoproterozoic and Palaeozoic—A Tale of Baltica and Laurentia. *Earth-Science Reviews*, 40(3/4): 229–258. [https://doi.org/10.1016/0012-8252\(96\)00008-6](https://doi.org/10.1016/0012-8252(96)00008-6)
- Villa, I. M., 1998. Isotopic Closure. *Terra Nova*, 10(1): 42–47. <https://doi.org/10.1046/j.1365-3121.1998.00156.x>
- Villa, I. M., 2006. From Nanometer to Megameter: Isotopes, Atomic-Scale Processes, and Continent-Scale Tectonic Models. *Lithos*, 87(3/4): 155–173. <https://doi.org/10.1016/j.lithos.2005.06.012>
- Villa, I. M., 2015.  $^{39}\text{Ar}$ - $^{40}\text{Ar}$  Geochronology of Mono- and Polymetamorphic Basement Rocks. *Periodico di Mineralogia*, 84: 615–632
- Villa, I. M., De Bièvre, P., Holden, N. E., et al., 2015. IUPAC-IUGS Recommendation on the Half Life of  $^{87}\text{Rb}$ . *Geochimica et Cosmochimica Acta*, 164: 382–385. <https://doi.org/10.1016/j.gca.2015.05.025>
- Waters, D. J., Martin, H. N., 1993. Geobarometry of Phengite-Bearing Eclogites. *Terra Abstracts*, 5: 410–411
- White, C. E., Barr, S. M., Jamieson, R. A., et al., 2001. Neoproterozoic High-Pressure/Low-Temperature Metamorphic Rocks in the Avalon Terrane, Southern New Brunswick, Canada. *Journal of Metamorphic Geology*, 19(5): 519–530. <https://doi.org/10.1046/j.0263-4929.2001.00326.x>
- Wijbrans, J. R., McDougall, I., 1986.  $^{40}\text{Ar}/^{39}\text{Ar}$  Dating of White Micas from an Alpine High-Pressure Metamorphic Belt on Naxos (Greece): The Resetting of the Argon Isotopic System. *Contributions to Mineralogy and Petrology*, 93(2): 187–194. <https://doi.org/10.1007/bf00371320>
- Willner, A. P., 2005. Pressure-Temperature Evolution of a Late Palaeozoic Paired Metamorphic Belt in North-Central Chile (34°–35°30'S). *Journal of Petrology*, 46(9): 1805–1833. <https://doi.org/10.1093/petrology/egi035>
- Willner, A. P., Ermolaeva, T., Stroink, L., et al., 2001. Contrasting Provenance Signals in Riphean and Vendian Sandstones in the SW Urals (Russia): Constraints for a Change from Passive to Active Continental Margin Conditions in the Neoproterozoic. *Precambrian Research*, 110(1/2/3/4): 215–239. [https://doi.org/10.1016/s0301-9268\(01\)00190-5](https://doi.org/10.1016/s0301-9268(01)00190-5)
- Willner, A. P., Gerdes, A., Massonne, H.-J., et al., 2014. Crustal Evolution of the Northeast Laurentian Margin and the Peri-Gondwanan Microcontinent Ganderia Prior to and during Closure of the Iapetus Ocean: Detrital Zircon U-Pb and Hf Isotope Evidence from Newfoundland. *Geoscience Canada*, 41(3): 345–361. <https://doi.org/10.12789/geocanj.2014.41.046>
- Willner, A. P., Sindern, S., Metzger, R., et al., 2002. Typology and Single Grain U/Pb Ages of Detrital Zircons from Proterozoic Sandstones in the SW Urals (Russia): Early Time Marks at the Eastern Margin of Baltica. *Precambrian Research*, 124(1): 1–20. [https://doi.org/10.1016/s0301-9268\(03\)00045-7](https://doi.org/10.1016/s0301-9268(03)00045-7)
- Willner, A. P., Thomson, S. N., Kröner, A., et al., 2005. Time Markers for the Evolution and Exhumation History of a Late Palaeozoic Paired Metamorphic Belt in North-Central Chile (34°–35°30'S). *Journal of Petrology*, 46(9): 1835–1858. <https://doi.org/10.1093/petrology/egi036>
- Willner, A. P., Wartho, J. A., Kramm, U., et al., 2004. Laser  $^{40}\text{Ar}/^{39}\text{Ar}$  Ages of Single Detrital White Mica Grains Related to the Exhumation of Neoproterozoic and Late Devonian High Pressure Rocks in the Southern Urals (Russia). *Geological Magazine*, 141(2): 161–172. <https://doi.org/10.1017/s0016756803008628>